HHS Public Access

Author manuscript

Mol Plant Microbe Interact. Author manuscript; available in PMC 2023 January 17.

Published in final edited form as:

Mol Plant Microbe Interact. 2022 December ; 35(12): 1067–1080. doi:10.1094/MPMI-05-22-0114-R.

Effectors from a Bacterial Vector-Borne Pathogen Exhibit Diverse Subcellular Localization, Expression Profiles, and Manipulation of Plant Defense

Paola A. Reyes Caldas[1], **Jie Zhu**[1], **Andrew Breakspear**[2], **Shree P. Thapa**[1], **Tania Y. Toruño**[1,3], **Laura M. Perilla-Henao**[1], **Clare Casteel**[1,4], **Christine R. Faulkner**[2], **Gitta Coaker**[1,†]

[1]Plant Pathology Department, University of California, Davis, CA, U.S.A.

[2]The John Innes Centre, Norwich Research Park, Norwich, U.K.

[3]Rijk Zwaan Breeding B.V, Burgemeester Crezéelaan 40, De Lier, 2678 KX, The Netherlands

[4]School of Integrative Plant Science, Plant-Microbe Biology and Plant Pathology Section, Cornell University, Ithaca, NY, U.S.A.

Abstract

Climate change is predicted to increase the prevalence of vector-borne disease due to expansion of insect populations. '*Candidatus* Liberibacter solanacearum' is a phloem-limited pathogen associated with multiple economically important diseases in solanaceous crops. Little is known about the strategies and pathogenicity factors '*Ca*. L. solanacearum' uses to colonize its vector and host. We determined the '*Ca*. L. solanacearum' effector repertoire by predicting proteins secreted by the general secretory pathway across four different '*Ca*. L. solanacearum' haplotypes, investigated effector localization in planta, and profiled effector expression in the vector and host. The localization of '*Ca*. L. solanacearum' effectors in *Nicotiana* spp. revealed diverse eukaryotic subcellular targets. The majority of tested effectors were unable to suppress plant immune responses, indicating they possess unique activities. Expression profiling in tomato and the psyllid *Bactericera cockerelli* indicated '*Ca*. L. solanacearum' differentially interacts with its host and vector and can switch effector expression in response to these environments. This study reveals '*Ca*. L. solanacearum' effectors possess complex expression patterns, target diverse host organelles and the majority are unable to suppress host immune responses. A mechanistic understanding of '*Ca*. L. solanacearum' effector function will reveal novel targets and provide insight into phloem biology.

Keywords

Candidatus Liberibacter solanacearum; phloem-limited pathogen; plant immunity; SEC effector; vector-borne disease

†Corresponding author: G. Coaker; glcoaker@ucdavis.edu.

***e*-Xtra:** Supplementary material is available online.

The author(s) declare no conflict of interest.

Vector-borne diseases (VBDs) reduce agricultural productivity and disrupt ecosystems worldwide. Rising global temperatures are predicted to increase insect populations and fitness, exacerbating the dispersion of emergent VBDs (Deutsch et al. 2018). Some of the most widespread and devastating VBDs are associated with '*Candidatus* Liberibacter' species, which are gram-negative, obligate, phloem-limited bacterial pathogens that are transmitted by different psyllid vectors onto plant hosts (Perilla-Henao and Casteel 2016). Huanglongbing disease, also known as citrus greening, is primarily associated with '*Candidatus* Liberibacter asiaticus' and is considered the most important citrus disease worldwide (Singerman and Rogers 2020). '*Candidatus* Liberibacter solanacearum' is associated with economically important diseases on a variety of solanaceous and apiaceous hosts, including tomato (tomato psyllid yellows) and potato (zebra chip).

Piercing-sucking insects, such as psyllids, insert their stylet into plant hosts and probe the apoplast as well as other cell types before reaching the phloem. During probing, insects secrete watery saliva containing herbivore-associated molecular patterns and other pathogen-associated molecular patterns derived from bacteria present in their body or salivary glands (Chaudhary et al. 2014; Jaouannet et al. 2014). Phloem responses to biotic stress or insect damage include the accumulation of nitric oxide (NO), reactive oxygen species (ROS), and Ca^{2+}, which are required for rapid systemic signaling. NO and ROS are required for the establishment of systemic acquired resistance, while a calcium-ROS autopropagation wave interacts with electric signals for induction of systemic wound responses (Gaupels et al. 2016, 2017). ROS and Ca^{2+} influx in vascular bundles leads to activation of occlusion proteins, callose deposition, and phytoalexin accumulation (Huang et al. 2020).

Plant pathogens rely on secretion of proteins called effectors that modify their host. '*Ca*. Liberibacter' species lack specialized secretion systems for specific delivery of effector proteins into host cells but harbor all the essential components of the general secretion pathway (SEC) for delivery to the bacterial periplasm. '*Ca*. Liberibacter' SEC effectors are secreted when using *Escherichia coli* as a surrogate (Prasad et al. 2016). Noncanonical secretion of periplasmic '*Ca*. Liberibacter' proteins likely occurs through outer membrane vesicles (OMVs), as OMVs have been well-characterized as an alternative route for secretion from the bacterial periplasm and have been visualized in '*Ca*. L. solanacearum' (Jonca et al. 2021; Solé et al. 2015; Nissinen et al. 2014). Noncanonical effector secretion was demonstrated using heterologous expression of two '*Ca*. L. asiaticus' proteins (CLIBASIA_RS0045 and SC2_gp095) in the culturable surrogate '*Ca*. L. crescens' (Jain et al. 2015, 2018, 2019). Predicted '*Ca*. L. asiaticus' effectors are small, which predicts their ability to move symplastically in planta away from the sieve elements through plasmodesmata. SDE1, a small secreted '*Ca*. L. asiaticus' effector protein, moves far from the point of infection, either by phloem transport or cell-to-cell movement through plasmodesmata (Pagliaccia et al. 2017). Phytoplasmas, another class of insect-vectored phloem-limited bacterial pathogens, also secrete effectors that move through plasmodesmata to manipulate their host (Tomkins et al. 2018).

To date, only a handful of '*Ca*. Liberibacter' effectors from any species have been characterized. '*Ca*. L. asiaticus' SEC-dependent effector 1 (SDE1) is preferentially expressed in citrus and periwinkle hosts, suppresses plant defense by targeting plant immune

proteases, and transgenic plants expressing SDE1 phenocopy leaf blotchy mottle disease symptoms (Clark et al. 2018, 2020; Pagliaccia et al. 2017). '*Ca*. L. asiaticus' SDE15 and '*Ca*. L. solanacearum' hypothetical protein effector 1 (HPE1) were also reported to suppress plant cell death (Levy et al. 2019; Pang et al. 2020). Phytoplasma effectors such as TENGU and SAP11 target transcription factors involved in the production of phytohormones, inducing disease phenotypes such as witche's broom and flower sterility in addition to impairing plant defenses and vector performance (Dermastia 2019; Sugio et al. 2011b; Tan et al. 2016). Despite the importance of bacterial effectors in promoting vector-borne disease development, little is known about the identity, conservation, and role of '*Ca*. L. solanacearum' effectors. Breakthroughs in understanding '*Ca*. Liberibacter' pathogenicity mechanisms could be achieved using '*Ca*. L. solanacearum' as a model system due to the ability to study disease in *Nicotiana tabacum*, *Nicotiana benthamiana*, and *Solanum lycopersicum* (tomato) (Huang et al. 2021).

'*Ca*. L. solanacearum' is the most recently evolved species within the '*Ca*. Liberibacter' genus and is divided into 12 haplotypes with different vector and host preferences; three are associated with diseases in solanaceous plants (haplotypes A, B, and F) and six are reported in a wide range of apiaceous crops (haplotypes C, D, E, H, Cras1, and Cras2) (Sumner-Kalkun et al. 2020; Thapa et al. 2020). '*Ca*. L. solanacearum' haplotypes cause different symptomatology (Mendoza-Herrera et al. 2018). '*Ca*. L. solanacearum' haplotypes A and B are capable of systemically colonizing and propagating in both vector (*Bactericera cockerelli*) and host (tomato and potato). Because of their inability to be cultured and their specific phloem localization, understanding the etiology and biology of the diseases caused by '*Ca*. Liberibacter' species has been challenging (Huang et al. 2020). Currently, there is no genetic resistance in cultivated plant germplasm and increasing resistance to insecticides pose a high risk for disease epidemics (Chávez et al. 2015; Szczepaniec et al. 2019).

Here, we studied '*Ca*. L. solanacearum' effectors to gain insight into disease development. SEC-secreted effectors were identified from four different '*Ca*. L. solanacearum' haplotypes. '*Ca*. L. solanacearum' effector localization was analyzed after transient expression in *Nicotiana* spp. We evaluated the ability of '*Ca*. L. solanacearum' effectors to suppress early markers of plant defense in response to perception of pathogen features. Despite diverse subcellular localizations, most tested effectors were unable to suppress host immune responses, indicating they possess unique activities. Expression profiling in tomato and the psyllid *B. cockerelli* highlighted three patterns of effector expression, i.e., early and late acting effectors, preferential expression in the vector or host, and constitutive effector expression across vector and host. This study highlights promising '*Ca*. L. solanacearum' effectors for future investigation.

Results

The '*Ca*. L. solanacearum' SEC effector repertoire varies in size and composition.

To begin investigating how '*Ca*. L. solanacearum' is able to colonize two distinct organisms and thrive in the phloem environment, we predicted suites of SEC-dependent effectors across four haplotypes (haplotypes A to D). '*Ca*. L. solanacearum' genomes were downloaded from the National Center for Biotechnology Information (NCBI) database,

including three from haplotype A (LsoNZ1, HenneA, R1), two from haplotype C (FIN111 and FIN114), and one from haplotypes B and D (‘*Ca*. L. solanacearum’ ZC1 and ISR100, respectively) (Fig. 1A) (Lin et al. 2011; Thompson et al. 2015; Wang et al. 2017; Zheng et al. 2014). Genome CP002371.1 (‘*Ca*. L. solanacearum’ ZC1) is completely finished, while the others are draft. SEC-dependent effectors were predicted using SignalP and were filtered to remove proteins with predicted transmembrane domains. The majority of ‘*Ca*. L. solanacearum’ secreted proteins are small, with sizes ranging between 10 to 20 kDa. We sought to produce a stringent list of potential mobile effectors; therefore, predicted secreted proteins were further filtered to remove those unable to move by simple diffusion through mesophyll plasmodesmata (>35 kDa) (Oparka et al. 1999; Kim et al. 2005). Only 20% of the predicted proteins were larger than 35 kDa, and their annotation suggested they have functions in bacterial replication, transport, and metabolism rather than host or vector modification. We found 13 effectors that are conserved in all the haplotypes screened (core) and 27 that were found in several but not all haplotypes (variable). Each haplotype carried between 27 to 36 predicted effectors (Supplementary Table S1), with haplotypes C and D having the smallest (27 to 29) and haplotypes A and B having the largest (34 to 36) repertoires (Fig. 1B). In total, we estimate the repertoire of effectors across ‘*Ca*. L. solanacearum’ haplotypes to be approximately 27, comprising 13 core, six variable, and eight unique effectors (Fig. 1B). These estimates could change with the sequencing of new strains and haplotypes.

Next, we analyzed effector conservation across ‘*Ca*. L. solanacearum’ haplotypes. None of the identified effectors share over 44% amino acid identity with proteins outside of their genus, indicating that they are unique to genus ‘*Ca*. Liberibacter’ and their function cannot be predicted by homology. Only one effector, HPE74, possessed an identifiable domain, Cupredoxin_1 domain PF13473 (Supplementary Table S1), which is predicted to bind a type I copper redox site and is involved in electron transfer reactions (Dennison 2013). To better understand the role of effector repertoires in the context of phylogenetic relationships, we performed phylogenetic analyses of ‘*Ca*. L. solanacearum’ haplotypes using 825 orthologous genes and compared them with phylogeny generated from the 13 core effectors (Fig. 1D). In general, the topology of both trees was similar. Analyses of variable and core effectors across haplotypes revealed that haplotypes A and B and haplotypes C and D are the most similar to each other (Fig. 1C and E), which is incongruent with their phylogeny but does coincide with their host range (Fig. 1D and E). We observed variation at the nucleotide level for the same effector between haplotypes (Fig. 1E). For example, HPE2, which is a core effector, possesses 80 to 93% amino acid similarity between haplotypes. It is possible that the combination of genome reduction associated with intracellular lifestyle, high AT content, and continuing expansion of ‘*Ca*. Liberibacter’ spp. geographical range are driving these observations.

‘*Ca*. L. solanacearum’ SEC effectors localize to different host compartments.

Haplotypes A and B possess a similar repertoire of effectors and exhibit similar host range, causing disease in potato and tomato (Fig. 1B to E). Haplotype B is more aggressive on both tomato and potato (Wen et al. 2013). Therefore, we focused on SEC-dependent effectors shared between haplotypes A and B (Fig. 1C) or unique for haplotype B.

To gain insight into the possible role of '*Ca*. L. solanacearum' SEC-dependent effectors, we evaluated their subcellular localization by fusing the mature effector (without signal peptide) with an N- terminal turboGFP (tGFP) tag using Golden Gate technology (Fig. 2A; Supplementary Fig. S1). turboGFP is a copGFP variant with more rapid folding and increased fluorescence (Shagin et al. 2004). tGFP-mEffector fusions were visualized by confocal microscopy using *Agrobacterium*-mediated transient expression in *Nicotiana benthamiana*. Effector expression was verified using anti-tGFP immunoblot (Supplementary Fig. S2). We were able to detect full-length protein expression for most of the effectors tested (Supplementary Fig. S2). We were unable to detect green fluorescent protein (GFP) expression for five effectors using anti-tGFP immunoblot but were able to visualize them by confocal microscopy (HPE2, HPE7, HPE16, HPE21, and HPE73) (Supplementary Figs. S1 and S2, data not shown).

HPE13 and HPE21 are present in a genomic island that is unique to haplotype B and exhibit different subcellular localizations (Supplementary Table S1). We observed HPE13 in the plasma membrane (PM) (Fig. 2B). To confirm HPE13 membrane localization, we induced plasmolysis with 1 M NaCl and were able to observe Hechtian strands stretching between the PM and the cell wall in tGFP-HPE13–expressing cells (Fig. 2B, right panel). Hechtian strands are thread-like structures formed by stretched PM in plasmolyzed cells that connect the plant cell wall and PM. To further confirm the localization of HPE13, we co-expressed tGFP-HPE13 with the PM aquaporin marker *AtPIP2A*-mCherry. To confirm the colocalization of HPE13, we plotted the intensity profiles of each fluorophore across a linear section and overlapping fluorescence intensity profiles confirmed the colocalization of HPE13 with the PM marker (Fig. 2C). Bacteria occasionally hijack the palmitoylation machinery of the host cell and undergo lipidation to accumulate in membranes. HPE13 was predicted, by GPS-Palm, to have an S-palmoytilation site in the C terminus (Ning et al. 2021). This post-translational modification may target HPE13 to plant membranes.

In contrast to HPE13, HPE21 targets a eukaryotic organelle. HPE21 localized to punctate structures that were ubiquitously distributed in the cytoplasm. HPE21 did not co-localize with a Golgi marker (soybean α-1,2-mannosidase I) (Supplementary Fig. S3). Instead HPE21 targeted peroxisomes as indicated by co-localization with 1-PTS1 peroxisomal-targeted mCherry (Fig. 2D). To confirm the colocalization of HPE21, we plotted the intensity profiles of each fluorophore across a linear section, as shown in Figure 2D. The intensity profiles of tGFP-HPE21 and the peroxisome marker matched exactly. HPE9 accumulated in the perinuclear membrane, a known site of endoplasmic reticulum (ER) accumulation (Perkins and Allan 2021), where the ER marker SP-mCherry-HDEL also accumulates (Fig. 2E). tGFP-HPE9 mainly co-localizes with SP-mCherry-HDEL throughout the cell, although there are some differences in the patterns of each protein. For example, SP-mCherry-HDEL is in the ER lumen, while HPE9 associates with the cytosolic face of the ER membrane. Altogether, these results suggest '*Ca*. L. solanacearum' effectors target specific eukaryotic subcellular compartments.

'*Ca*. L. solanacearum' effectors target specific subnuclear compartments.

Multiple phytoplasma effectors target plant nuclei to reprogram their hosts (Tomkins et al. 2018). We were keen to understand if nuclear targeting is a common strategy among phloem-limited plant-pathogenic bacteria. Seven proteins encoded a monopartite or bipartite nuclear localization signal (NLS), namely, HPE2, HPE8, HPE9, HPE15, HPE16, HPE22, and HPE30 (Fig. 3; Supplementary Fig. S1). However, only four effectors exhibited exclusive nuclear localization, i.e., HPE16, HPE18, HPE19, and HPE73 (Fig. 3C; Supplementary Fig. S1). HPE18 is found in haplotypes A, B, and D, HPE19 is found exclusively in haplotypes B and D, and HPE8, HPE16, and HPE73 are core effectors (Supplementary Table S1). HPE8 preferentially accumulates in the nucleus but is also found in the cytoplasm (Fig. 3B). Interestingly, we found HPE16 present in fast-moving punctate bodies inside the nucleus (Fig. 3C; Supplementary Video S1). These structures, known as nuclear speckles, are important for RNA metabolism and possibly facilitate regulation of gene expression (Bazin et al. 2018; Reddy et al. 2012). HPE18 accumulates in the nucleolus, while HPE73 accumulates in both the nucleus and nucleolus (Supplementary Fig. S1B). The majority of '*Ca*. L. solanacearum' effector proteins, 16 of 23 tested effectors, exhibited nuclear cytoplasmic localization (Figs. 3 and 4; Supplementary Fig. S1). Five effectors exhibited sole or predominant nuclear localization. These data highlight the importance of effector nuclear targeting in '*Ca*. Liberibacter' species.

'*Ca*. L. solanacearum' HPE19 targets nuclei and chloroplasts.

Investigating HPE19 localization was challenging due to low-level expression. To enhance HPE19 expression, we cloned HPE19 with a tGFP tag under a dexamethasone (Dex)-inducible GAL4 promoter and induced expression with Dex 12 h postinfiltration (hpi). tGFP-HPE19 expressed under an inducible promoter revealed differences in its subcellular localization over time. At 24 hpi, we observed nuclear localized HPE19 (Fig. 4A). However, fluorescence was detected primarily in chloroplasts and stromule-like projections 48 hpi (Fig. 4B, panel inset). HPE19 chloroplast localization was supported by overlapping tGFP fluorescence and chloroplast autofluorescence intensity profiles across a linear section at 48 hpi but not at 24 hpi (Fig. 4A and B, right panels). Strikingly, chloroplast showing tGFP-HPE19 fluorescence were also observed in nearby nuclei (Fig. 4C, right panel). A three-dimensional (3D) reconstruction of 20 images found that chloroplasts completely surround tGFP-HPE19 positive but not control tGFP nuclei (Fig. 4D). Clustering of chloroplasts around nuclei has been observed in plant-pathogen interactions and is believed to be important for plant defense activation (Ding et al. 2019; Krenz et al. 2012; Park et al. 2018a). Next, we investigated if expression of HPE19 induces plant cell death, a common defense response. Expression of HPE19 under a 35S constitutive or GAL4 inducible promoter did not induce a visible cell death (Fig. 4E). Trypan blue vital staining revealed expression of HPE19 in *N. benthamiana* does not induce microscopic cell death. To confirm these results, we measured electrolyte ion leakage and were not able to detect any increase in ion leakage, a hallmark of cell death, after expression of HPE19 (Fig. 4F). Expression of the pro-apoptotic protein BAX was able to induce visible cell death, cell death stained by trypan blue, and electrolyte leakage (Fig. 4E and F). However, HPE19 slightly enhanced ROS and Ca^{2+} production in response to chitin perception (Fig. 6). Contrary to our expectations, HPE19 suppressed ROS production in response to flg22, indicating this

effector does not universally enhance plant responses to all pathogen features (Fig. 6). It is possible that tGFP-HPE19 weakly activates plant defense or alters other processes, resulting in stress response.

'*Ca*. L. solanacearum' SEC-dependent effectors are able to move cell-to-cell.

'*Ca*. L. solanacearum' is a phloem-limited bacterial pathogen and is confined to sieve elements (Secor et al. 2009). Sieve elements are metabolically inactive enucleated cells that heavily rely on companion cells for their function. The specific localization of '*Ca*. L. solanacearum' effectors in eukaryotic compartments indicates these proteins can move to companion cells and other neighboring cell types to target host compartments. To determine the ability of '*Ca*. L. solanacearum' effectors to move intercellularly, mature '*Ca*. L. solanacearum' effectors were C-terminally fused to enhanced green fluorescent protein (eGFP) and co-expressed with nuclear tdTomato (Fig. 5A). As a positive control, we co-expressed the highly mobile eGFP with nuclear tdTomato. As a negative control, we co-expressed the nonmobile 2xeGFP with nuclear tdTomato. NLS-tdTomato and the 2xeGFP control are too large to diffuse cell-to-cell. A low concentration of *Agrobacterium tumefaciens* was used to facilitate single-cell transformation. Effector mobility was observed 24 h after *Agrobacterium*-mediated transient expression in epidermal cells of *N. benthamiana*. Cell-to-cell movement was visualized in cells with green fluorescence surrounding an original transformation event. A clear positive result for this assay requires robust effector expression.

We were able to detect movement of two out of five tested '*Ca*. L. solanacearum' effectors (HPE1, HPE8, HPE9, HPE16, HPE19). Of 11 isolated single cell transformation events, we observed eight (72.7%) instances of HPE1 movement to adjacent cells (Fig. 5B; Supplementary Fig. S4). HPE1 was previously characterized as a plant cell-death suppressor (Levy et al. 2019). We also observed movement of HPE8, which accumulates highly in the nucleus and is easy to visualize. Of 11 isolated single cell transformation events, we observed 10 (90.9%) instances of HPE8 movement to adjacent cells (Fig. 5B; Supplementary Fig. S4). Differences in the size of HPE1 and HPE8 (11.32 and 8.78 kDa, respectively) could account for the more limited movement of HPE1. Only 16.7% positives were observed for the 2xeGFP negative control, and 100% positives were observed for the eGFP positive control, indicating that the movement system is working properly. These data provide evidence that a subset of '*Ca*. L. solanacearum' effectors are capable of cell-to-cell movement.

The majority of '*Ca*. L. solanacearum' SEC-dependent effectors do not suppress plant immunity.

The most well-characterized function of pathogen effectors is their ability to suppress defense responses (Toruño et al. 2016). Insect feeding not only elicits wound-associated responses, but their saliva and honeydew also carries insect and microbial features associated with plant pathogens and symbionts that can trigger a defense response (Huang et al. 2020). We investigated the ability of '*Ca*. L. solanacearum' effectors to suppress plant immune defenses. To investigate immune suppression, we analyzed two early defense hallmarks of plant immunity, i.e., Ca^{2+} influx and production of ROS. These two responses also comprise

the main events shaping subsequent defense responses reported in phloem (Gaupels et al. 2016, 2017).

We evaluated effector-mediated suppression of plant immune responses to two pathogen features, flg22 and chitin. Flg22 is an immunogenic peptide of flagellin perceived by the surface-localized receptor FLS2. Chitin is an oligosaccharide present in the cell walls of fungi and exoskeletons of insects that is perceived by LysM domain–containing surface-localized immune receptors. Cytosolic Ca^{2+} accumulation was quantified in a transgenic *N. benthamiana* aequorin reporter line (Segonzac et al. 2011). '*Ca*. L. solanacearum' effectors were transiently expressed along with tGFP in *N. benthamiana*; 24 h later, leaf tissue was collected and floated on coelenterezine solution for at least 12 h and was challenged with chitin or flg22. We analyzed ten effectors representing different subcellular localizations (Figs. 3, 4, and 6; Supplementary Fig. S1). Surprisingly, '*Ca*. L. solanacearum' effectors failed to suppress the intracellular accumulation of Ca^{2+} upon perception of flg22 or chitin (Fig. 6A and C). Only HPE16 was able to inhibit the Ca^{2+} influx after chitin challenge. Several effectors increased Ca^{2+} influx upon perception of either flg22 (HPE8, HPE13) or chitin (HPE21) (Fig. 6A and C). While some effectors displayed a similar trend of increased Ca^{2+} influx, these results were not statistically significant.

Next, we examined whether '*Ca*. L. solanacearum' effectors alter ROS production in response to perception of flg22 and chitin. '*Ca*. L. solanacearum' effectors were infiltrated along with tGFP and were transiently expressed in *N. benthamiana*, and, 24 h later, leaf tissue was collected, was floated in water overnight, and was challenged with either immunogenic feature. In general, most tested effectors failed to suppress the ROS production elicited by either flg22 (Fig. 6B) or chitin (Fig. 6D). Only three effectors consistently inhibited ROS production (Fig. 6B and D). HPE16 suppresses chitin-induced ROS and Ca^{2+} influx but does not significantly alter flg22-induced responses (Fig. 6). HPE19 was able to suppress flg22-induced ROS but slightly enhanced ROS and Ca^{2+} influx after chitin treatment (Fig. 6). Differential suppression of flg22 and chitin immune outcomes have been reported for *Pseudomonas syringae* type III effectors (Gimenez-Ibanez et al. 2018). '*Ca*. L. solanacearum' effectors involved in plant immune suppression may target different immune signaling components. Altogether these data indicate that the majority of '*Ca*. L. solanacearum' effectors are not capable of suppressing plant immune hallmarks. This pattern is strikingly different compared with the extensive defense-suppressing effector activity of other gram-negative foliar pathogens, including *P. syringae* (Guo et al. 2009).

Differential expression of '*Ca*. L. solanacearum' effectors in the plant and the vector.

Insect-vectored plant pathogens must be able to adapt to two drastically different environments, their vector and their host. '*Ca*. L. solanacearum' SEC-dependent effectors likely contribute to the ability to colonize plant sieve elements and propagate in *B. cockerelli*. We hypothesized that '*Ca*. L. solanacearum' expresses different suites of effectors in vector and host, which can provide insight into contribution of specific effectors in disease development. We investigated the expression of '*Ca*. L. solanacearum' effectors in tomato and in *B. cockerelli* using one-step reverse transcription-quantitative PCR (RT-qPCR). Synchronized *B. cockerelli* colonies infected with haplotype B were used to transmit

‘*Ca*. L. solanacearum’ onto tomato cultivar MoneyMaker (Fig. 7A). Psyllids were kept in a muslin bag and, 72 h after vector transmission, were removed for RNA extraction. Midribs were extracted from the original inoculated leaf one month postinoculation. Up- and downregulated genes in each treatment were identified after normalizing to the ‘*Ca*. L. solanacearum’ housekeeping gene *glnA*. We were able to identify five effectors that are strongly expressed in tomato one month postinoculation compared with the psyllid (HPE2, HPE3, HPE16, HPE27, HPE74) (Fig. 7B). We also identified five effectors that are strongly expressed in the psyllid compared with tomato (HPE4, HPE6, HPE15, HPE18, HPE33). Nine effectors were more uniformly expressed in both organisms (Fig. 7B). Collectively, these data support the hypothesis that some ‘*Ca*. L. solanacearum’ effectors are required for eukaryotic colonization, but other suites of effectors are differentially deployed to manipulate the host and vector.

In infected plants, ‘*Ca*. Liberibacter’ distribution and titers and disease symptoms are patchy and variable from plant-to-plant (Li et al. 2009b). We also observed differences in ‘*Ca*. L. solanacearum’ titers between plant samples in which cycle threshold (Ct) values of the ‘*Ca*. L. solanacearum’ housekeeping gene *recA* at week 1 varied between 26.89 and 34.0 and, at week 4, varied between 22.74 and 24.61. ‘*Ca*. Liberibacter’ infection is characterized by an asymptomatic period followed by the development of disease. In addition, disease symptoms can take months to years to develop, depending on the plant host. Due to the long latent period for disease development, we hypothesize that ‘*Ca*. L. solanacearum’ differentially expresses effectors depending on infection stage. To this end, we also compared effector expression in tomato at 1 and 4 weeks after vector transmission.

Although there was variation between biological samples, we identified sets of early- and late-acting (Fig. 7C, top and middle panels, respectively) effectors. Interestingly, most late-acting effectors are core effectors (Fig. 7C). In general, HPE74 and HPE30 exhibited reproducible expression and were highly upregulated at 1 week, while HPE2 and HPE8 were reproducibly downregulated at 4 weeks after vector transmission (Fig. 7C). These results demonstrate that over the course of infection the effector expression profile shifts, potentially enabling adaptation to new environments.

Discussion

VBDs significantly impact agricultural production and are important emerging diseases. Despite the importance of VBDs, scientists do not have a robust understanding of host manipulation regulated by vector-borne pathogens compared with foliar pathogens (Huang et al. 2020; Perilla-Henao and Casteel 2016). Some of the most important bacterial vector-borne pathogens reside in the ‘*Ca*. Liberibacter’ genus, including the devastating citrus pathogen ‘*Ca*. L. asiaticus’ and the solanaceous and apiaceous pathogen ‘*Ca*. L. solanacearum’. In this study, we analyzed the identity, localization, defense suppression, and expression of ‘*Ca*. L. solanacearum’ haplotype A and B effectors. Our results show ‘*Ca*. L. solanacearum’ effectors target diverse eukaryotic subcellular compartments, are capable of moving cell-to-cell, and exhibit complex expression patterns in vector and host. Most ‘*Ca*. L. solanacearum’ effectors do not suppress host immune responses, indicating that they have novel targets, potentially related to VBD spread.

Vector-borne plant pathogens must exhibit high transcriptional flexibility in order to adapt to distinct organisms, insect and plant. Bacterial effector expression is known to be hierarchical, but there is little evidence of dynamic expression patterns during the course of plant bacterial infection (Lara-Tejero et al. 2011; Mills et al. 2008; Portaliou et al. 2017). Filamentous pathogens are known to express waves of effectors during infection. For example, the hemibiotrophic fungal pathogen *Colletotrichum higginsianum* expresses specific sets of effectors during pre-penetration, biotrophic, and necrotrophic infection stages (Kleemann et al. 2012). Similarly, we observed '*Ca*. L. solanacearum' effectors exhibit dynamic expression profiles in tomato, identifying sets of early and late expressed effectors (Fig. 7C). '*Ca*. L. solanacearum'–infected tomato plants show symptoms starting five weeks after –vector transmission (Mendoza-Herrera et al. 2018) Therefore, late acting effectors could play an important role in disease symptomatology and acquisition, while early effectors could act in transmission or manipulating the phloem environment for bacterial proliferation. The plant distribution and titer of '*Ca*. L. solanacearum' is patchy (Li et al. 2009a). If '*Ca*. L. solanacearum' effector expression is density-dependent, this could explain the observed variability in effector expression across samples. Differences in effector expression were also observed between tomato and psyllid (Fig. 7B), indicating that '*Ca*. L. solanacearum' utilizes its effector repertoire to adapt to diverse environments. Several '*Ca*. L. asiaticus' effectors also show differential expression in their host and vectors as well as different host genotypes, but dynamics during infection have not been studied (Clark et al. 2018; Liu et al. 2019; Pagliaccia et al. 2017; Yan et al. 2013). Our results suggest '*Ca*. L. solanacearum' requires a specific set of effectors to interact with the plant at different stages of the infection and core effectors, which are predominantly expressed during late stages of infection, most likely play a role in disease development.

'*Ca*. L. solanacearum' SEC effectors target several subcellular compartments that are absent in bacteria, including the ER, peroxisomes, chloroplasts, and nuclei (Figs. 2, 3, and 4); these compartments are known targets of plant-pathogen effectors (Park et al. 2018b; Toruño et al. 2016). SEC effector targeting of eukaryotic compartments indicates they function outside of the bacterium to modulate host and vector. In addition, we found '*Ca*. L. solanacearum' effectors can move cell-to-cell (Fig. 5), indicating they are capable of movement during infection. Effector mobility has been observed in other vascular (*Fusarium oxysporum* in tomato) and nonvascular (*Magnaporte oryzae* in rice) pathosystems (Cao et al. 2018; Khang et al. 2010). Movement of effectors might be particularly important for phloem-limited pathogens to thrive. Multiple phytoplasma SEC-dependent effectors are mobile, target transcription factors, and influence disease symptomology and transmission (Tomkins et al. 2018). '*Ca*. L. solanacearum' HPE16 localizes to nuclear speckles (Fig. 3C), a site of storage for RNA metabolism proteins, including transcription factors (Bazin et al. 2018). There are a few examples of effectors targeting this compartment, including PsAvh52, a *Phytophthora sojae* effector, that induces transcriptional reprogramming by recruiting a plant transacetylase to nuclear speckles (Li et al. 2018). Further characterization of the plant targets of mobile, nuclear-localized effectors will reveal if targeting of transcription factors is a common mechanism for phloem-limited pathogens.

Plants rely on surface-localized receptors to recognize pathogens, including insects, and are activated upon insect feed and salivary secretions in the apoplast. Phloem defense responses

include the production of ROS, Ca^{2+} influx, callose deposition, and activation of proteins capable of occluding sieve elements (Huang et al. 2020). However, a detailed mechanistic understanding of phloem-mediated defense remains elusive. Watery saliva of aphids and leafhoppers contain effectors that suppress plant recognition, demonstrating the importance of plant immunity against VBD (Huang et al. 2020). Transcriptional profiling in tomato has revealed that '*Ca*. L. solanacearum' haplotype B–infected plants exhibit downregulation of defense-related genes during the initial stages of infection (Casteel et al. 2012; Huot et al. 2018). The nuclear effectors HPE16 and HPE19 as well as the nuclear-cytoplasmic effector HPE2 were successful at suppressing one or both cytosolic Ca^{2+} accumulation and ROS production (Fig. 6). Effector tagging can impair protein functionality. Thus, future studies utilizing C-terminal tags or untagged effectors may reveal additional phenotypes. '*Ca*. L. solanacearum' HPE1 was previously reported as a variable BAX-induced cell death and Prf hypersensitive response (HR) suppressor (Levy et al. 2019). Plants infected with '*Ca*. L. solanacearum' usually contains high amounts of ROS and other defense-related compounds (Kumar et al. 2017; Wallis et al. 2012); the fact that we could not find more effectors that consistently suppress ROS production upon perception of pathogen features could partially explain the high accumulation of these compounds. The '*Ca*. L. asiaticus' SEC effector SDE1 promotes plant defense suppression by targeting plant immune proteases in the phloem (Clark et al. 2018). '*Ca*. L. asiaticus' SDE15 is a broad defense suppressor that inhibits HR induced by *Xanthomonas citri* pv. *citri* in citrus (Pang et al. 2020). Although multiple '*Ca*. L. asiaticus' SEC effectors have been investigated, only two (SDE1 and SDE15) have been demonstrated to suppress plant immunity (Clark et al. 2018; Pang et al. 2020). Similarly, in this study we found the majority of '*Ca*. L. solanacearum' SEC-dependent effectors fail to suppress early hallmarks of defense (Fig. 6). These results suggest genus '*Ca*. Liberibacter' only requires a few effectors for defense suppression.

Extracellular bacteria must overcome a multilayered plant defense before being able to establish disease; therefore, the majority of their effectors are involved in plant immunity suppression (Guo et al. 2009; Medina et al. 2018; Traore et al. 2019). In contrast, phloem-limited pathogens are deposited directly inside plant cells, escaping apoplastic defense. This protective intracellular niche could explain the low number of SEC-dependent effectors in phytoplasmas and '*Ca*. Liberibacter' species reported in plant defense suppression (Clark et al. 2018; Pang et al. 2020; Sugio et al. 2011a; Wang et al. 2018). Other vector-borne pathogens manipulate their hosts for transmission. For example, the *Turnip mosaic virus* and *Potato virus Y* use NIaPro, a protease with dynamic vacuolar localization, to increase vector performance and suppress aphid-induced callose deposition (Bak et al. 2017; Casteel et al. 2015). Because phloem-limited pathogens cannot colonize a new host by themselves, it is likely '*Ca*. L. solanacearum' effectors play a role in modifying their environment and facilitating transmission.

Here, we initiated the characterization of '*Ca*. L. solanacearum' effectors. The interaction of '*Ca*. L. solanacearum' with solanaceous plants, including tomato and potato, is economically important and represents a more tractable system to investigate VBD and unravel novel phloem-specific defense strategies. This study sets the stage for future mechanistic investigation of '*Ca*. L. solanacearum' effector targets.

Materials and Methods

Plant materials and growing conditions.

Nicotiana benthamiana wild type and transgenic line SRLJ15 expressing aequorin (Segonzac et al. 2011) plants were grown in a controlled environment chamber at 26°C and 12-h light and 12-h dark photoperiod with light intensity of 180 μE m^{-2} s^{-1}. Tomato plants (*Solanum lycopersicum* cv. Money Maker) were grown under controlled conditions at 26°C and 12-h light and 12-h dark photoperiod. *B. cockerelli* psyllids carrying '*Ca*. L. solanacearum' haplotype B of the Western biotype were reared in tomato plants inside a 60×60×60 cm Bugdorm insect-rearing cage (BioQuip Products). All experiments were performed using synchronized colonies. To synchronize *B. cockerelli* colonies, 15 to 20 adult psyllids were collected from infected symptomatic or clean plants and were transferred to healthy 5-week-old tomato plants inside a 24.5×24.5×63 cm Bugdorm insect-rearing cage (BioQuip Products). At 72 h postinfestation, the adult psyllids were removed and the plants were kept 21 to 26 days until new adults emerged.

Effector prediction.

'*Ca*. L. solanacearum' genomes for haplotype A (JQIG01, JMTK01, JNVH01), B (CP002371.1), C (LVWB01, LVWE01), and D (LLVZ01) were used to predict secreted proteins with a signal peptide, using SignalP v3.0 and v4.1 (Bendtsen et al. 2004; Petersen et al. 2011). Proteins larger than 35 kDa and containing predicted transmembrane domains (TMHMM v2.0) (Krogh et al. 2001) were removed.

Effector conservation analyses were performed in pairwise comparisons, using BLASTP and BLASTN (Gish et al. 1990). The threshold of percent similarity for presence and absence was 40%. The presence of eukaryotic NLSs was predicted using the LOCALIZER web server (Sperschneider et al. 2017). All predicted effectors are listed in Supplementary Table S1.

Phylogenetic analysis.

Orthologous genes of '*Ca*. L. solanacearum' isolates were predicted using the OrthoMCL v. 2.0 pipeline (Li et al. 2003). All-versus-all BLASTN comparison of all gene sequences for each species was performed and orthologous genes were clustered by OrthoMCL v. 2.0. Multiple alignments of gene sequences were performed with PRANK 170427 (Löytynoja 2014). All the alignments were concatenated by FASconCAT v. 1.1, yielding a gene supermatrix (Kück and Meusemann 2010). A maximum-likelihood approach was used to reconstruct the phylogenetic tree, using RAxML v. 8.2 software (Stamatakis 2014). The bootstrap was performed with 1,000 replicates. The resulting tree was visualized using FigTree v. 1.4.3.

Effector cloning.

To create N-terminal fusions with tGFP or C-terminal fusions with eGFP, we used the Golden Gate toolkit for plants (Engler et al. 2014). '*Ca*. L. solanacearum' mature effectors (without signal peptide) were amplified from haplotype A and B–infected tomato genomic DNA, under standard PCR conditions, using iProof (Bio-Rad) (Supplementary Table S1).

Annealing temperatures of primer pairs were calculated using Fast-PCR (Kalendar et al. 2011). Amplicons of the expected size were purified and subcloned in the respective level zero acceptor for CDS1ns or CDS2 parts (Supplementary Table S3). Effector clones were confirmed by PCR and sequencing. To generate the fluorophore-tagged fusions, confirmed effectors were cloned in the Golden Gate level 2 acceptor plasmid pICH86966, using a restriction-ligation reaction. To assess symplastic mobility of '*Ca*. L. solanacearum' effectors, a new Golden Gate vector (FP08018-BsaI) was engineered. The vector contains a constitutively expressed, cell-to-cell immobile, nuclear localized tdTomato (transformation control) as well as a 35S promoter-*lacZ*-eGFP cassette. The *lacZ* is flanked by *Bsa*I recognition sites, allowing PCR-amplified '*Ca*. L. solanacearum' effectors to be introduced with a Golden Gate reaction. The vector was produced using Golden Gate assembly of pre-existing basic parts (Engler et al. 2014) and newly created level 0 modules for *lacZ* and tdTomato. Control constructs containing nuclear localized tdTomato and a mobile eGFP (FP08024) or immobile 2XeGFP (FP08027) were also produced using Golden Gate assembly. Effector clones were confirmed by PCR, restriction digestion, and sequencing. Final constructs were transformed in *A. tumefaciens* GV3101. HPE19 was subcloned in the entry vector pENTR/SD/D-TOPO, following manufacturer instructions and was cloned into the destination vector pTA7001(Li et al. 2013) using a Gateway LR reaction (Invitrogen). Sequences of destination vector inserts were confirmed and then transformed in *A. tumefaciens* GV3101. All primers used for cloning are listed in Supplementary Table S2, plasmids are listed in Supplementary Table S3, and effectors are listed in Supplementary Table S1.

Western blotting.

To evaluate '*Ca*. L. solanacearum' effector expression, individual effectors were cloned at tGFP fusions and expressed in *N. benthamiana* using *Agrobacterium*-mediated transient expression. *A. tumefaciens* GV3101 carrying effectors was induced with 100 μM acetosyringone for 1 h and was infiltrated at an optical density at 600 nm (OD_{600}) = 0.5. Total protein was isolated from *N. benthamiana* leaves 24 hpi by grinding in 2× Laemmli buffer (Laemmli 1970). Protein samples were separated by sodium dodecyl sulfate-polyacrylamide gel electrophoresis and immunoblotting was conducted, using anti-tGFP at a concentration of 1:10,000 (Invitrogen), followed by secondary anti–rabbit-HRP (horseradish peroxidase) at a concentration of 1:3,000 (Bio-Rad). Positive signals were detected via chemiluminescence, using the Super Signal West Femto Chemiluminescent Substrate (Pierce), and were visualized using the Bio-Rad Chemidoc system.

Confocal microscopy and effector mobility.

A. tumefaciens GV3101 carrying effectors was induced with 100 μM acetosyringone for 1 h and was infiltrated at an OD_{600} = 0.5 into *N. benthamiana*. Imaging was performed at 24 hpi. Plasmolysis was performed using 1 M NaCl. Specific mCherry markers for the PM (pm-rkCD3–1007), ER (ER-rk CD3–959), Golgi (G-rkCD3–967), and peroxisome (px-rk CD3–983) were mixed in a 1:1 ratio with '*Ca*. L. solanacearum'–tagged effectors, were co-infiltrated in *N. benthamiana*, and were visualized at 48 hpi. All confocal microscopy was performed using a Leica SP8 confocal scope equipped with a 63× water objective. tGFP was excited at 488 nm, and the emission was gathered at 500 to 550 nm. mCherry was excited

at 550 nm and the emission gathered at 570 to 600 nm. The chloroplast autofluorescence emission was gathered at 650 to 750 nm. Images were analyzed using the Leica Application Suite X (LASX) software, 3D reconstructions were generated using the 3D visualization and analyses tools in the LAS X Core module.

For effector mobility assays, *A. tumefaciens* GV3101 carrying HPE1-eGFP, HPE8-eGFP, pF08024 (eGFP), and pF08027 (2xeGFP) (Supplementary Table S3) were infiltrated at an OD_{600} = 0.0005. Imaging was performed at 48 hpi, using a Leica SP8 confocal scope. eGFP was excited at 488 nm, and the emission was gathered at 495 to 540 nm. tdTomato was excited at 552 nm, and the emission was gathered at 561 to 616 nm. Single transformation events were observed with a 20× objective in a Leica SP8 confocal scope.

Trypan blue staining and electrolyte leakage assay.

N. benthamiana leaves were infiltrated with *A. tumefaciens* GV3101 carrying either t-GFP, tGFP-HPE19, or BAX as described above. Twenty-four hours later, leaves were infiltrated with 2 μM Dex for GAL4 promoter constructs. Leaves were detached 5 days after *Agrobacterium*-mediated transient expression and were subjected to trypan blue staining and destained with chloral hydrate (1.25 g/ml), as previously described (McDowell et al. 2011). Electrolyte leakage was measured as previously described (Bolus et al. 2019). Samples from the different treatments were collected using a number 9 cork borer (0.79 cm^2) 12 h after Dex induction. Individual leaf discs were placed in a 12-well tissue culture plate with 5 ml of distilled water for 30 min. Water was replaced with 2 ml of distilled water, and leaf discs were kept at room temperature under constant 30 μmol s^{-1} m^{-2} light. Conductivity (microsiemens per centimeter) was measured using a Model 3200 conductance instrument (YSI) every 24 h for five days. Statistical differences were detected using a repeated measures analysis of variance and different groups were assigned using Tukey's post-hoc test.

ROS burst and cytosolic calcium accumulation assay.

N. benthamiana wild type at the two-leaf stage was inoculated with *Agrobacterium tumefaciens* GV3010 at an OD_{600} = 0.5 containing the mature effector side by side with the control *Agrobacterium tumefaciens* GV3010 containing an empty vector (EV). For ROS, leaf discs were excised with a number 1 cork borer (0.48 cm^2) at 24 hpi and were incubated overnight in water. Before measurement, the water was removed and 100 μl of assay solution (17 mM luminol, 1 μM HRP, and 100 nM flg22 (Genescript) or 100 μg of chitin hexamers per milliliter (Megazyme) was added to each well. Transient increase of cytosolic Ca^{2+} concentration was monitored in the *N. benthamiana* SLJR15 line (Segonzac et al. 2011). Leaf discs were excised at 24 hpi and were incubated overnight in 1 μM native coelenterazin (Sigma). Before measurement, the solution was removed and 100 μl of assay solution (100 nM flg22 or 100 μg of chitim per milliliter) was added to each well. Luminescence was measured using a TriStar Luminometer. Experiments included three biological replicates (individual plants) and were repeated three times (n = 9 plants). Statistical differences in ROS production or calcium accumulation were detected using multiple Mann-Whitney tests. Adjusted P values from the Holm-Sidak method were used to compute adjusted P values. Outliers were detected by the ROUT method and were removed from the analyses.

Timecourse expression analyses of '*Ca*. L. solanacearum' effectors in tomato and psyllid.

Three-week-old tomato *Solanum lycopersicum* cv. Money Maker plants were infected under controlled conditions with 15 newly emerged psyllids from a synchronized '*Ca*. L. solanacearum' haplotype B colony. Psyllids were confined in a muslin bag, were removed after 72 h, were flash-frozen in liquid nitrogen, and were stored at −80°C until RNA extraction. The leaves were inspected and eggs (if present) were carefully removed using tape. Midvein samples (about 50 mg) were collected from the originally inoculated leaves at 1 or 4 weeks post–vector transmission. Six individual plants were included per experimental timepoint. Fifteen recovered psyllids were pooled for RNA extraction per infected plant. Total RNA was isolated, using the TRIzol reagent (Invitrogen) following manufacturer instructions. To guarantee DNA removal, an additional cleaning step with acid phenol was added before precipitation of the RNA by adding an equal volume of acid-phenol:chloroform 5:1 solution, pH 4.5 (Ambion). Total RNA was quantified with a Nanodrop 2000 spectrophotometer (Thermo Scientific). The '*Ca*. L. solanacearum' titer for each sample was assessed using the RecA primers (Ibanez et al. 2014), and the three samples with the best Ct values for each timepoint were selected for further analysis.

The iTaq Universal SyberGreen One-Step RT-qPCR kit (Bio-rad) was used to perform RT-qPCR, following manufacturer protocol. One microliter of a 1:2 dilution of RNA (about 100 to 250 ng) was used per reaction. Effector expression was quantified on the CFX96 real-time PCR detection system (Bio-Rad). Gene expression was calculated using the ΔCt method and was normalized against the *GlnA* housekeeping gene. Primers were designed with Primer3 (Untergasser et al. 2012) and are provided in Supplementary Table S4. Pheatmap R package was used for plotting the histograms and performing hierarchical clustering (Kolde 2012).

Supplementary Material

Refer to Web version on PubMed Central for supplementary material.

Funding:

This material is based upon work supported by the National Institutes of Health under grant number R35GM136402 and the United States Department of Agriculture National Institute of Food and Agriculture grant number 2019-70016-2979 awarded to G. Coaker. P. Reyes Caldas and L. M. Perilla-Henao were supported by a Fulbright Columbia Fellowship. C. R. Faulkner and A. Breakspear were supported by grants from the Biotechnology and Biological Research Council (BBS/E/J/000PR9796) and the European Research Council (725459, "INTERCELLAR"). C. Casteel was supported by startup funds from the University of California Davis and National Science Foundation grant number 1723926.

Data availability.

Genome and effector sequences are available from NCBI using the accession numbers provided in Supplementary Table S1. All other raw data are available upon request from the corresponding author.

Literature Cited

Bak A, Cheung AL, Yang C, Whitham SA, and Casteel CL 2017. A viral protease relocalizes in the presence of the vector to promote vector performance. Nat. Commun 8:14493.

Bazin J, Romero N, Rigo R, Charon C, Blein T, Ariel F, and Crespi M 2018. Nuclear speckle RNA binding proteins remodel alternative splicing and the non-coding Arabidopsis transcriptome to regulate a cross-talk between auxin and immune responses. Front. Plant Sci 9:1209. [PubMed: 30186296]

Bendtsen JD, Nielsen H, Von Heijne G, and Brunak S 2004. Improved prediction of signal peptides: SignalP 3.0. J. Mol. Biol 340:783–795. [PubMed: 15223320]

Bolus S, Akhunov E, Coaker G, and Dubcovsky J 2019. Dissection of cell death induction by wheat stem rust resistance protein Sr35 and its matching effector AvrSr35. Mol. Plant-Microbe Interact 33:308–319. [PubMed: 31556346]

Cao L, Blekemolen MC, Tintor N, Cornelissen BJC, and Takken FLW 2018. The *Fusarium oxysporum* Avr2-Six5 effector pair alters plasmodesmatal exclusion selectivity to facilitate cell-to-cell movement of Avr2. Mol. Plant 11:691–705. [PubMed: 29481865]

Casteel CL, De Alwis M, Bak A, Dong H, Whitham SA, and Jander G 2015. Disruption of ethylene responses by *Turnip mosaic virus* mediates suppression of plant defense against the green peach aphid vector. Plant Physiol 169:209–218. [PubMed: 26091820]

Casteel CL, Hansen AK, Walling LL, and Paine TD 2012. Manipulation of plant defense responses by the tomato psyllid (*Bactericerca cockerelli*) and its associated endosymbiont *Candidatus* Liberibacter psyllaurous. PLoS One 7:e35191.

Chaudhary R, Atamian HS, Shen Z, Briggs SP, and Kaloshian I 2014. GroEL from the endosymbiont *Buchnera aphidicola* betrays the aphid by triggering plant defense. Proc. Natl. Acad. Sci. U. S. A 111: 8919–8924. [PubMed: 24927572]

Chávez EC, Bautista OH, Flores JL, Uribe LA, and Fuentes YMO 2015. Insecticide-resistance ratios of three populations of *Bactericera cockerelli* (Hemiptera: Psylloidea: Triozidae) in regions of northern Mexico. Florida Entomol 98:950–953.

Clark K, Franco JY, Schwizer S, Pang Z, Hawara E, Liebrand TWH, Pagliaccia D, Zeng L, Gurung FB, Wang P, Shi J, Wang Y, Ancona V, van der Hoorn RAL, Wang N, Coaker G, and Ma W 2018. An effector from the huanglongbing-associated pathogen targets citrus proteases. Nat. Commun 9:1718. [PubMed: 29712915]

Clark KJ, Pang Z, Trinh J, Wang N, and Ma W 2020. Sec-delivered effector 1 (SDE1) of '*Candidatus* Liberibacter asiaticus' promotes citrus huanglongbing. Mol. Plant-Microbe Interact 33:1394–1404. [PubMed: 32986514]

Dennison C 2013. Cupredoxins BT. Pages 404–406 in: Encyclopedia of Biophysics Roberts GCK, ed. Springer, Berlin.

Dermastia M 2019. Plant hormones in phytoplasma infected plants. Front.Plant Sci 10:477. [PubMed: 31057582]

Deutsch CA, Tewksbury JJ, Tigchelaar M, Battisti DS, Merrill SC, Huey RB, and Naylor RL 2018. Increase in crop losses to insect pests in a warming climate. Science 361:916–919. [PubMed: 30166490]

Ding X, Jimenez-Gongora T, Krenz B, and Lozano-Duran R 2019. Chloroplast clustering around the nucleus is a general response to pathogen perception in *Nicotiana benthamiana*. Mol. Plant Pathol 20:1298–1306. [PubMed: 31257720]

Engler C, Youles M, Gruetzner R, Ehnert T-M, Werner S, Jones JDG, Patron NJ, and Marillonnet S 2014. A Golden Gate modular cloning toolbox for plants. ACS Synth. Biol 3:839–843. [PubMed: 24933124]

Gaupels F, Durner J, and Kogel K-H 2017. Production, amplification and systemic propagation of redox messengers in plants? The phloem can do it all! New Phytol 214:554–560. [PubMed: 28044323]

Gaupels F, Furch ACU, Zimmermann MR, Chen F, Kaever V, Buhtz A, Kehr J, Sarioglu H, Kogel K-H, and Durner J 2016. Systemic induction of NO-, redox-, and cGMP signaling in the pumpkin extrafascicular phloem upon local leaf wounding. Front. Plant Sci 7:154. [PubMed: 26904092]

Gimenez-Ibanez S, Hann DR, Chang JH, Segonzac C, Boller T, and Rathjen JP 2018. Differential Suppression of *Nicotiana benthamiana* innate immune responses by transiently expressed *Pseudomonas syringae* type III effectors. Front. Plant Sci 9:688. [PubMed: 29875790]

Gish W, Altschul SF, Lipman DJ, Miller W, and Myers EW 1990. Basic local alignment search tool. J. Mol. Biol 215:403–10. [PubMed: 2231712]

Guo M, Tian F, Wamboldt Y, and Alfano JR 2009. The majority of the type III effector inventory of *Pseudomonas syringae* pv. *tomato* DC3000 can suppress plant immunity. Mol. Plant. Microbe. Interact 22: 1069–1080. [PubMed: 19656042]

Huang CY u, Niu D, Kund G, Jones M, Albrecht U, Nguyen L, Bui C, Ramadugu C, Bowman KD, Trumble J, and Jin H 2021. Identification of citrus immune regulators involved in defence against huanglongbing using a new functional screening system. Plant Biotechnol. J 19:757–766. [PubMed: 33108698]

Huang W, Reyes-Caldas P, Mann M, Seifbarghi S, Kahn A, Almeida RPP, BÃ©ven L, Heck M, Hogenhout SA, and Coaker G 2020. Bacterial vector-borne plant diseases: Unanswered questions and future directions. Mol. Plant 13:1379–1393. [PubMed: 32835885]

Huot OB, Levy JG, and Tamborindeguy C 2018. Global gene regulation in tomato plant (*Solanum lycopersicum*) responding to vector (*Bactericera cockerelli*) feeding and pathogen (‘*Candidatus* Liberibacter solanacearum’) infection. Plant Mol. Biol 97:57–72. [PubMed: 29619663]

Ibanez F, Levy J, and Tamborindeguy C 2014. Transcriptome analysis of “*Candidatus* Liberibacter solanacearum” in its psyllid vector, *Bactericera cockerelli*. PLoS One 9:e100955.

Jain M, Fleites LA, and Gabriel DW 2015. Prophage-encoded peroxidase in ‘*Candidatus* Liberibacter asiaticus’ is a secreted effector that suppresses plant defenses. Mol. Plant-Microbe Interact 28:1330–1337. [PubMed: 26313412]

Jain M, Munoz-Bodnar A, and Gabriel DW 2019. ‘*Candidatus* Liberibacter asiaticus’ peroxiredoxin (LasBCP) suppresses oxylipin-mediated defense signaling in citrus. J. Plant Physiol 236:61–65. [PubMed: 30884323]

Jain M, Munoz-Bodnar A, Zhang S, and Gabriel DW 2018. A secreted ‘*Candidatus* Liberibacter asiaticus’ peroxiredoxin simultaneously suppresses both localized and systemic innate immune responses in planta. Mol. Plant-Microbe Interact 31:1312–1322. [PubMed: 29953333]

Jaouannet M, Rodriguez PA, Thorpe P, Lenoir CJG, MacLeod R, Escudero-Martinez C, and Bos JIB 2014. Plant immunity in plantaphid interactions. Front. Plant Sci 5:663. [PubMed: 25520727]

Jonca J, Waleron M, Czaplewska P, Bogucka A, Steć A, Dziomba S, Jasiecki J, Rychłowski M, and Waleron K 2021. Membrane vesicles of *Pectobacterium* as an effective protein secretion system. Int. J. Mol. Sci 22:12574.

Kalendar R, Lee D, and Schulman AH 2011. Java web tools for PCR, in silico PCR, and oligonucleotide assembly and analysis. Genomics 98:137–144. [PubMed: 21569836]

Khang CH, Berruyer R, Giraldo MC, Kankanala P, Park S-Y, Czymmek K, Kang S, and Valent B 2010. Translocation of *Magnaporthe oryzae* effectors into rice cells and their subsequent cell-to-cell movement. Plant Cell 22:1388–1403. [PubMed: 20435900]

Kim I, Cho E, Crawford K, Hempel FD, and Zambryski PC 2005. Cell-to-cell movement of GFP during embryogenesis and early seedling development in *Arabidopsis*. Proc. Natl. Acad. Sci. U.S.A 102: 2227–2231. [PubMed: 15668382]

Kleemann J, Rincon-Rivera LJ, Takahara H, Neumann U, van Themaat EVL, van der Does HC, Hacquard S, Stüber K, Will I, Schmalenbach W, Schmelzer E, and O’Connell RJ 2012. Sequential delivery of host-induced virulence effectors by appressoria and intracellular hyphae of the phytopathogen *Colletotrichum higginsianum*. PLOS Pathog 8:e1002643.

Kolde R 2012. Pheatmap: Pretty heatmaps. R package version 061 The R Foundation. Vienna.

Krenz B, Jeske H, and Kleinow T 2012. The induction of stromule formation by a plant DNA-virus in epidermal leaf tissues suggests a novel intra- and intercellular macromolecular trafficking route. Front. Plant Sci 3:291. [PubMed: 23293643]

Krogh A, Larsson B, Von Heijne G, and Sonnhammer ELL 2001. Predicting transmembrane protein topology with a hidden Markov model: Application to complete genomes. J. Mol. Biol 305:567–580. [PubMed: 11152613]

Kück P, and Meusemann K 2010. FASconCAT: Convenient handling of data matrices. Mol. Phylogenet. Evol 56:1115–1118. [PubMed: 20416383]

Kumar GNM, Knowles LO, and Knowles NR 2017. Zebra chip disease enhances respiration and oxidative stress of potato tubers (*Solanum tuberosum* L.). Planta 246:625–639. [PubMed: 28623560]

Laemmli UK 1970. Cleavage of structural proteins during the assembly of the head of bacteriophage T4. Nature 227:680–685. [PubMed: 5432063]

Lara-Tejero M, Kato J, Wagner S, Liu X, and Galán JE 2011. A sorting platform determines the order of protein secretion in bacterial type III systems. Science 331:1188–1191. [PubMed: 21292939]

Levy JG, Gross R, Mendoza-Herrera A, Tang X, Babilonia K, Shan L, Kuhl JC, Dibble MS, Xiao F, and Tamborindeguy C 2019. Lso-HPE1, an effector of '*Candidatus* Liberibacter solanacearum', can repress plant immune response. Phytopathology 110:648–655.

Li H, Wang H, Jing M, Zhu J, Guo B, Wang Y, Lin Y, Chen H, Kong L, Ma Z, Wang Y, Ye W, Dong S, Tyler B, and Wang Y 2018. A *Phytophthora* effector recruits a host cytoplasmic transacetylase into nuclear speckles to enhance plant susceptibility. Elife 7: e40039.

Li L, Stoeckert CJ Jr, and Roos DS 2003. OrthoMCL: Identification of ortholog groups for eukaryotic genomes. Genome Res 13:2178–2189. [PubMed: 12952885]

Li W, Abad JA, French-Monar RD, Rascoe J, Wen A, Gudmestad NC, Secor GA, Lee I-M, Duan Y, and Levy L 2009a. Multiplex real-time PCR for detection, identification and quantification of '*Candidatus* Liberibacter solanacearum' in potato plants with zebra chip. J. Microbiol. Methods 78:59–65. [PubMed: 19409423]

Li W, Chiang Y-H, and Coaker G 2013. The HopQ1 effector's nucleoside hydrolase-like domain is required for bacterial virulence in *Arabidopsis* and tomato, but not host recognition in tobacco. PLoS One 8:e59684.

Li W, Levy L, and Hartung JS 2009b. Quantitative distribution of '*Candidatus* Liberibacter asiaticus' in citrus plants with citrus huanglongbing. Phytopathology 99:139–144. [PubMed: 19159305]

Lin H, Lou B, Glynn JM, Doddapaneni H, Civerolo EL, Chen C, Duan Y, Zhou L, and Vahling CM 2011. The complete genome sequence of "*Candidatus* Liberibacter solanacearum", the bacterium associated with potato zebra chip disease. PLoS One 6:e19135.

Liu X, Fan Y, Zhang C, Dai M, Wang X, and Li W 2019. Nuclear import of a secreted "*Candidatus* Liberibacter asiaticus" protein is temperature dependent and contributes to pathogenicity in *Nicotiana benthamiana*. Front. Microbiol 10:1684. [PubMed: 31396191]

Löytynoja A 2014. Phylogeny-aware alignment with PRANK. Pages 155–170 in: Multiple Sequence Alignment Methods. Methods in Molecular Biology Russell DJ, ed.: Humana Press, Totowa, NJ, U.S.A.

McDowell JM, Hoff T, Anderson RG, and Deegan D 2011. Propagation, storage, and assays with *Hyaloperonospora arabidopsidis*: A model oomycete pathogen of *Arabidopsis*. Pages 137–151 in: Plant Immunity. Methods in Molecular Biology McDowell JM, ed. Humana Press, Totowa, NJ, U.S.A.

Medina CA, Reyes PA, Trujillo CA, Gonzalez JL, Bejarano DA, Montenegro NA, Jacobs JM, Joe A, Restrepo S, Alfano JR, and Bernal A 2018. The role of type III effectors from *Xanthomonas axonopodis* pv. *manihotis* in virulence and suppression of plant immunity. Mol. Plant Pathol 19:593–606. [PubMed: 28218447]

Mendoza-Herrera A, Levy J, Harrison K, Yao J, Ibanez F, and Tamborindeguy C 2018. Infection by '*Candidatus* Liberibacter solanacearum' haplotypes A and B in *Solanum lycopersicum* 'Moneymaker.'. Plant Dis 102:2009–2015. [PubMed: 30133358]

Mills E, Baruch K, Charpentier X, Kobi S, and Rosenshine I 2008. Real-time analysis of effector translocation by the type III secretion system of enteropathogenic *Escherichia coli*. Cell Host Microbe 3: 104–113. [PubMed: 18312845]

Ning W, Jiang P, Guo Y, Wang C, Tan X, Zhang W, Peng D i, and Xue Y u 2021. GPS-Palm: A deep learning-based graphic presentation system for the prediction of *S*-palmitoylation sites in proteins. Brief. Bioinform 22:1836–1847. [PubMed: 32248222]

Nissinen AI, Haapalainen M, Jauhiainen L, Lindman M, and Pirhonen M 2014. Different symptoms in carrots caused by male and female carrot psyllid feeding and infection by '*Candidatus* Liberibacter solanacearum.' Plant Pathol 63:812–820.

Oparka KJ, Roberts AG, Boevink P, Santa Cruz S, Roberts I, Pradel KS, Imlau A, Kotlizky G, Sauer N, and Epel B 1999. Simple, but not branched, plasmodesmata allow the nonspecific trafficking of proteins in developing tobacco leaves. Cell 97:743–754. [PubMed: 10380926]

Pagliaccia D, Shi J, Pang Z, Hawara E, Clark K, Thapa SP, De Francesco AD, Liu J, Tran T-T, Bodaghi S, Folimonova SY, Ancona V, Mulchandani A, Coaker G, Wang N, Vidalakis G, and Ma W 2017. A pathogen secreted protein as a detection marker for citrus huanglongbing. Front. Microbiol 8:2041. [PubMed: 29403441]

Pang Z, Zhang L, Coaker G, Ma W, He S-Y, and Wang N 2020. Citrus CsACD2 is a target of *Candidatus* Liberibacter asiaticus in huanglongbing disease. Plant Physiol 184:792–805. [PubMed: 32759268]

Park E, Caplan JL, and Dinesh-Kumar SP 2018a. Dynamic coordination of plastid morphological change by cytoskeleton for chloroplast-nucleus communication during plant immune responses. Plant Signal. Behav 13:1.

Park E, Nedo A, Caplan JL, and Dinesh-Kumar SP 2018b. Plant-microbe interactions: Organelles and the cytoskeleton in action. New Phytol 217:1012–1028. [PubMed: 29250789]

Perilla-Henao LM, and Casteel CL 2016. Vector-borne bacterial plant pathogens: Interactions with hemipteran insects and plants. Front. Plant Sci 7:1163. [PubMed: 27555855]

Perkins HT, and Allan V 2021. Intertwined and finely balanced: Endoplasmic reticulum morphology, dynamics, function, and diseases. Cells10.

Petersen TN, Brunak S, Von Heijne G, and Nielsen H 2011. SignalP4.0: Discriminating signal peptides from transmembrane regions. Nat. Methods 8:785–786. [PubMed: 21959131]

Portaliou AG, Tsolis KC, Loos MS, Balabanidou V, Rayo J, Tsirigotaki A, Crepin VF, Frankel G, Kalodimos CG, Karamanou S, and Economou A 2017. Hierarchical protein targeting and secretion is controlled by an affinity switch in the type III secretion system of enteropathogenic *Escherichia coli*. EMBO J 36:3517–3531. [PubMed: 29109154]

Prasad S, Xu J, Zhang Y, and Wang N 2016. SEC-translocon dependent extracytoplasmic proteins of *Candidatus* liberibacter asiaticus. Front. Microbiol 7.

Reddy ASN, Day IS, Göhring J, and Barta A 2012. Localization and dynamics of nuclear speckles in plants. Plant Physiol 158:67–77. [PubMed: 22045923]

Secor GA, Rivera VV, Abad JA, Lee I-M, Clover GRG, Liefting LW, Li X, and De Boer SH 2009. Association of ‘ *Candidatus* Liberibacter solanacearum’ with zebra chip disease of potato established by graft and psyllid transmission, electron microscopy, and PCR. Plant Dis 93:574–583. [PubMed: 30764398]

Segonzac C, Feike D, Gimenez-Ibanez S, Hann DR, Zipfel C, and Rathjen JP 2011. Hierarchy and roles of pathogen-associated molecular pattern-induced responses in *Nicotiana benthamiana*. Plant Physiol 156:687–699. [PubMed: 21478366]

Shagin DA, Barsova EV, Yanushevich YG, Fradkov AF, Lukyanov KA, Labas YA, Semenova TN, Ugalde JA, Meyers A, Nunez JM, Widder EA, Lukyanov SA, and Matz MV 2004. GFP-like proteins as ubiquitous metazoan superfamily: evolution of functional features and structural complexity. Mol. Biol. Evol 21:841–850. [PubMed: 14963095]

Singerman A, and Rogers ME 2020. The economic challenges of dealing with citrus greening: The case of Florida. J. Integr. Pest Manag 11:3.

Solé M, Scheibner F, Hoffmeister A-K, Hartmann N, Hause G, Rother A, Jordan M, Lautier M, Arlat M, and Büttner D 2015. *Xanthomonas campestris* pv. *vesicatoria* secretes proteases and xylanases via the Xps type II secretion system and outer membrane vesicles. J. Bacteriol 197:2879–2893. [PubMed: 26124239]

Sperschneider J, Catanzariti A-M, DeBoer K, Petre B, Gardiner DM, Singh KB, Dodds PN, and Taylor JM 2017. LOCALIZER: Subcellular localization prediction of both plant and effector proteins in the plant cell. Sci. Rep 7:44598.

Stamatakis A 2014. RAxML version 8: A tool for phylogenetic analysis and post-analysis of large phylogenies. Bioinformatics 30:1312–1313. [PubMed: 24451623]

Sugio A, MacLean AM, Kingdom HN, Grieve VM, Manimekalai R, and Hogenhout SA 2011a. Diverse targets of phytoplasma effectors: From plant development to defense against insects. Annu. Rev. Phytopathol 49:175–195. [PubMed: 21838574]

Sugio A, Kingdom HN, MacLean AM, Grieve VM, and Hogenhout SA 2011b. Phytoplasma protein effector SAP11 enhances insect vector reproduction by manipulating plant development and defense hormone biosynthesis. Proc. Natl. Acad. Sci. U.S.A 108:e1254–e1263. [PubMed: 22065743]

Sumner-Kalkun JC, Highet F, Arnsdorf YM, Back E, Carnegie M, Madden S, Carboni S, Billaud W, Lawrence Z, and Kenyon D 2020. '*Candidatus* Liberibacter solanacearum' distribution and diversity in Scotland and the characterisation of novel haplotypes from *Craspedolepta* spp. (Psyllidae: Aphalaridae). Sci. Rep 10:16567.

Szczepaniec A, Varela KA, Kiani M, Paetzold L, and Rush CM 2019. Incidence of resistance to neonicotinoid insecticides in *Bactericera cockerelli* across Southwest U.S. Crop Prot 116:188–195.

Tan CM, Li C-H, Tsao N-W, Su L. i-W.,Lu Y-T, Chang SH, Lin Y. iY. u, Liou J-C, Hsieh L. i-C., Yu J.-Z. u, Sheue C-R, Wang S-Y, Lee C.-F. a, and Yang J.-Y. i 2016. Phytoplasma SAP11 alters 3-isobutyl-2-methoxypyrazine biosynthesis in *Nicotiana benthamiana* by suppressing NbOMT1. J. Exp. Bot 67:4415–4425. [PubMed: 27279277]

Thapa SP, De Francesco A, Trinh J, Gurung FB, Pang Z, Vidalakis G, Wang N, Ancona V, Ma W, and Coaker G 2020. Genome-wide analyses of *Liberibacter* species provides insights into evolution, phylogenetic relationships, and virulence factors. Mol. Plant Pathol 21:716–731. [PubMed: 32108417]

Thompson SM, Johnson CP, Lu AY, Frampton RA, Sullivan KL, Fiers MWEJ, Crowhurst RN, Pitman AR, Scott IAW, Wen A, Gudmestad NC, and Smith GR 2015. Genomes of '*Candidatus* Liberibacter solanacearum' haplotype A from New Zealand and the United States suggest significant genome plasticity in the species. Phytopathology 105:863–871. [PubMed: 25822188]

Tomkins M, Kliot A, Marée AF, and Hogenhout SA 2018. A multilayered mechanistic modelling approach to understand how effector genes extend beyond phytoplasma to modulate plant hosts, insect vectors and the environment. Curr. Opin. Plant Biol 44:39–48. [PubMed: 29547737]

Toruño TY, Stergiopoulos I, and Coaker G 2016. Plant-pathogen effectors: Cellular probes interfering with plant defenses in spatial and temporal manners. Annu. Rev. Phytopathol 54:419–441. [PubMed: 27359369]

Traore S. y M., Eckshtainâ Levi N, Miao J, Castro Sparks A, Wang Z, Wang K, Li Q. i, Burdman S, Walcott R, Welbaum GE, and Zhao B 2019. *Nicotiana* species as surrogate host for studying the pathogenicity of *Acidovorax citrulli*, the causal agent of bacterial fruit blotch of cucurbits. Mol. Plant Pathol 20:800–814. [PubMed: 30938096]

Untergasser A, Cutcutache I, Koressaar T, Ye J, Faircloth BC, Remm M, and Rozen SG 2012. Primer3—New capabilities and interfaces. Nucleic Acids Res 40:e115–e115. [PubMed: 22730293]

Wallis CM, Chen J, and Civerolo EL 2012. Zebra chip-diseased potato tubers are characterized by increased levels of host phenolics, amino acids, and defense-related proteins. Physiol. Mol. Plant Pathol 78:66–72.

Wang J, Haapalainen M, Schott T, Thompson SM, Smith GR, Nissinen AI, and Pirhonen M 2017. Genomic sequence of '*Candidatus* Liberibacter solanacearum' haplotype C and its comparison with haplotype A and B genomes. PLoS One 12:e0171531.

Wang N, Li Y, Chen W, Yang HZ, Zhang PH, and Wu YF 2018. Identification of wheat blue dwarf phytoplasma effectors targeting plant proliferation and defence responses. Plant Pathol 67:603–609.

Wen A, Johnson C, and Gudmestad NC 2013. Development of a PCR assay for the rapid detection and differentiation of '*Candidatus* Liberibacter solanacearum' haplotypes and their spatiotemporal distribution in the United States. Am. J. Potato Res 90:229–236.

Yan Q, Sreedharan A, Wei S, Wang J, Pelz-Stelinski K, Folimonova S, and Wang N 2013. Global gene expression changes in *Candidatus* Liberibacter asiaticus during the transmission in distinct hosts between plant and insect. Mol. Plant Pathol 14:391–404. [PubMed: 23336388]

Zheng Z, Clark N, Keremane M, Lee R, Wallis C, Deng X, and Chen J 2014. Whole-genome sequence of '*Candidatus* Liberibacter solanacearum' strain R1 from California. Genome Announc 2: e01353–14. [PubMed: 25540355]

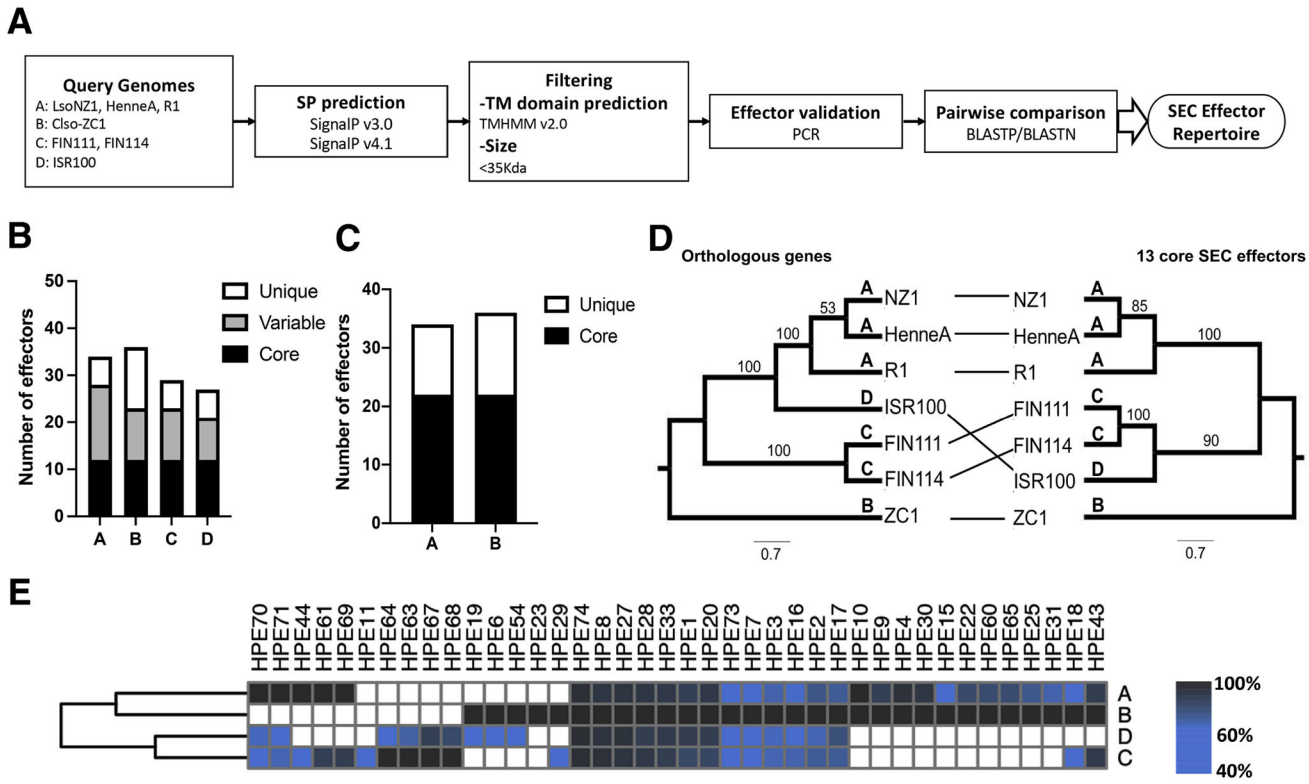

Fig. 1.

Prediction and classification of '*Candidatus* Liberibacter solanacearum' secretion pathway (SEC)-dependent effectors. **A**, Pipeline used to predict the '*Ca*. L. solanacearum' effector repertoire. '*Ca*. L. solanacearum' genomes for haplotypes A (JQIG01, JMTK01, JNVH01), B (CP002371.1), C (LVWB01, LVWE01), and D (LLVZ01) were used to predict secreted proteins with a signal peptide (SP). Proteins larger than 35 kDa and containing predicted transmembrane (TM) domains were removed. Effectors were PCR-validated in haplotypes A (LsoNZ1) and B (CLso_NZ1). **B**, '*Ca*. L. solanacearum' effectors were classified into three categories, i.e., those present in all haplotypes (core), those shared only with one or two haplotypes (variable), and those unique to each haplotype. **C**, Effector repertoire comparison across multiple strains of haplotypes A and B. The criteria and genomes utilized are the same as in B. **D**, Left: '*Ca*. L. solanacearum' phylogeny based on 815 orthologous genes. Right: '*Ca*. L. solanacearum' phylogeny based on the 13 core effectors. A maximum likelihood approach was used to generate each phylogeny with 1,000 bootstrap replicates. Bootstrap values are indicated at each node. **E**, Presence and absence hierarchical clustered heatmap of effectors found in at least two haplotypes. Colors represent percent amino acid identity across rows. Haplotypes are shown to the right.

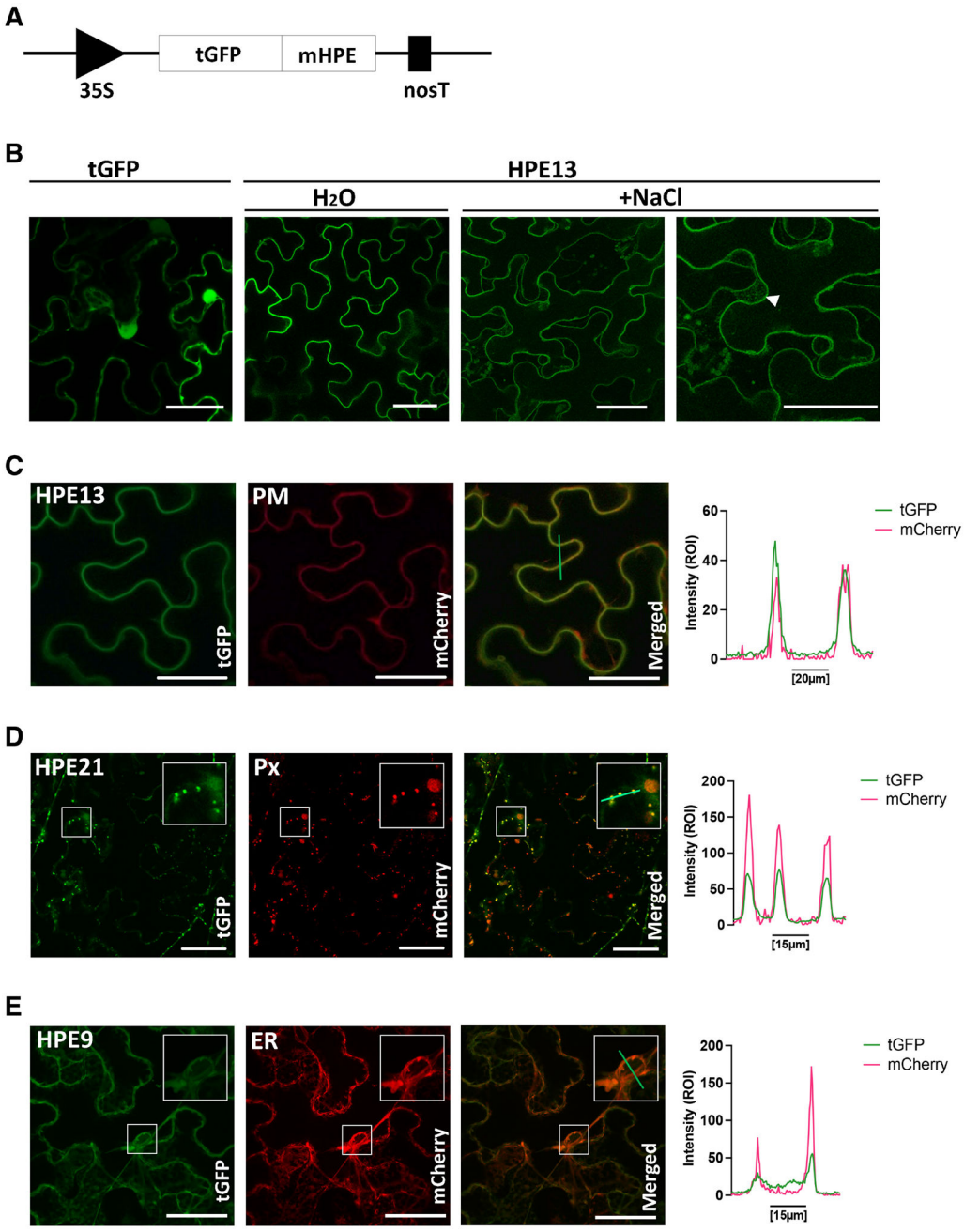

Fig. 2.

'*Candidatus* Liberibacter solanacearum' effectors localize to specific plant subcellular compartments. **A**, Mature effectors (mEffector) lacking their N-terminal signal peptide were cloned with an N-terminal fusion to TurboGFP (tGFP) and were visualized by confocal microscopy 24 h after transient expression in *Nicotiana benthamiana*. **B**, tGFP-HPE13 localizes to the plasma membrane (PM). Leaves expressing HPE13 were subjected to plasmolysis with 1 M NaCl for 30 min, the arrow indicates Hechtian strands. Leaves infiltrated with water were used as a control. **C**, tGFP-HPE13(left) was co-infiltrated with *AtPIP2A*-mCherry (center). Right panel shows the intensity profile for the green line in the

merged image. **D**, tGFP-HPE21(left) was co-infiltrated with 1-PTS1 peroxisomal-targeted mCherry (center). Inset in the right panel is a close-up of the colocalization of tGFP-HPE21 with peroxisomes in the merged image. Right panel shows the intensity profile for the green line in the merged image. **E**, tGFP-HPE9 was co-expressed with a SP-mCherry-HDEL labeling the endoplasmic reticulum (ER). Inset in the right panel is a close-up of the colocalization of tGFP-HPE9 with the ER in the merged image. Right panel shows the intensity profile for the green line in the merged image. Bars = 50 μm.

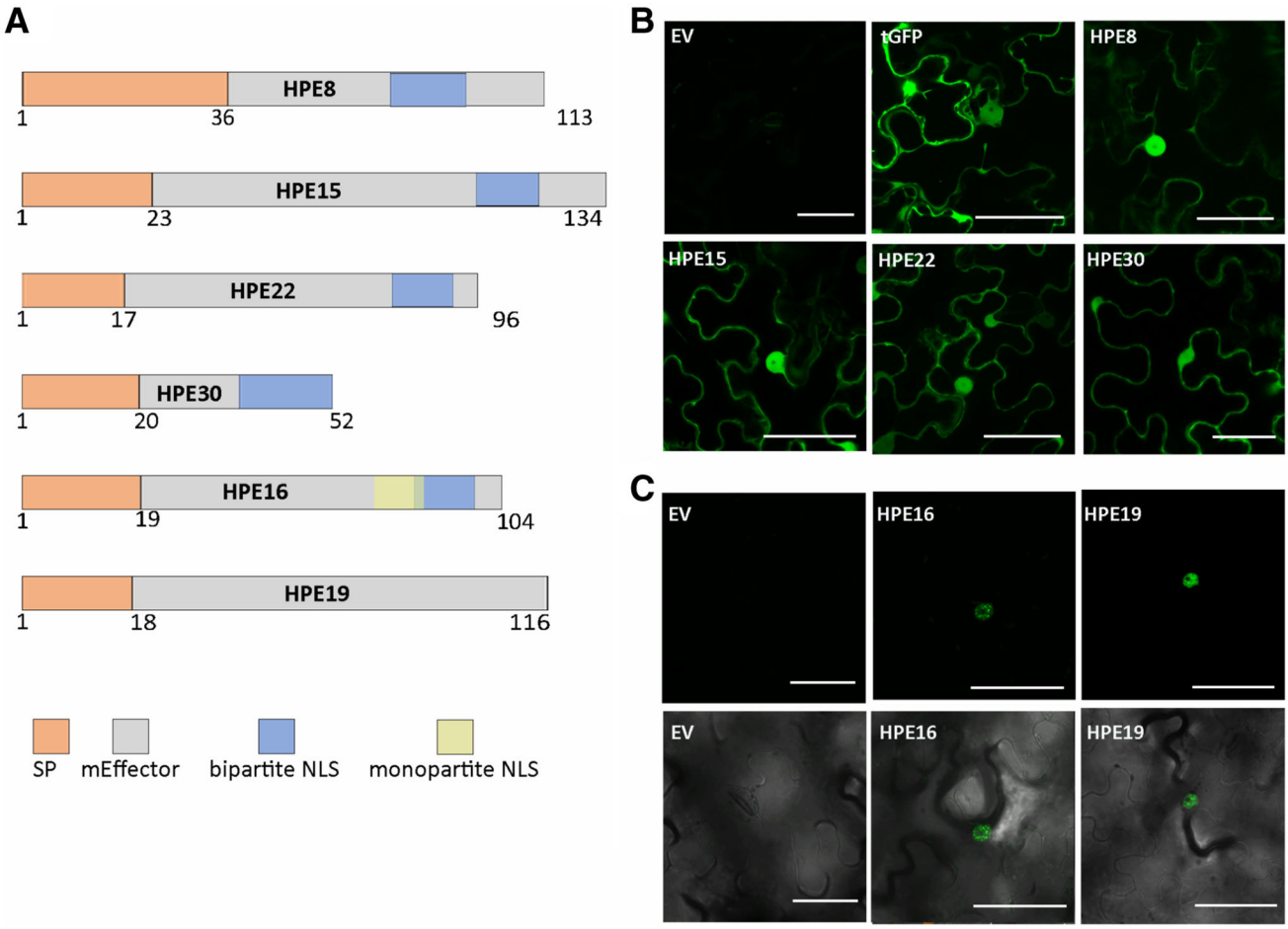

Fig. 3.

Multiple '*Candidatus* Liberibacter solanacearum' effectors localize to the nucleus and cytoplasm in planta. Mature effectors (mEffector) lacking their N-terminal signal peptide were cloned with an N-terminal fusion to TurboGFP (tGFP) and were visualized by confocal microscopy 24 h after transient expression in *Nicotiana benthamiana*. **A**, Schematic representation of '*Ca*. L. solanacearum' effectors including predicted nuclear localization signals (NLS). **B**, The majority of '*Ca*. L. solanacearum' effectors exhibited a nuclear and cytoplasmic localization (16 of 23 tested). **C**, HPE16 and HPE19 exhibit nuclear localization, bottom panel merged with bright field. Bars = 50 μm.

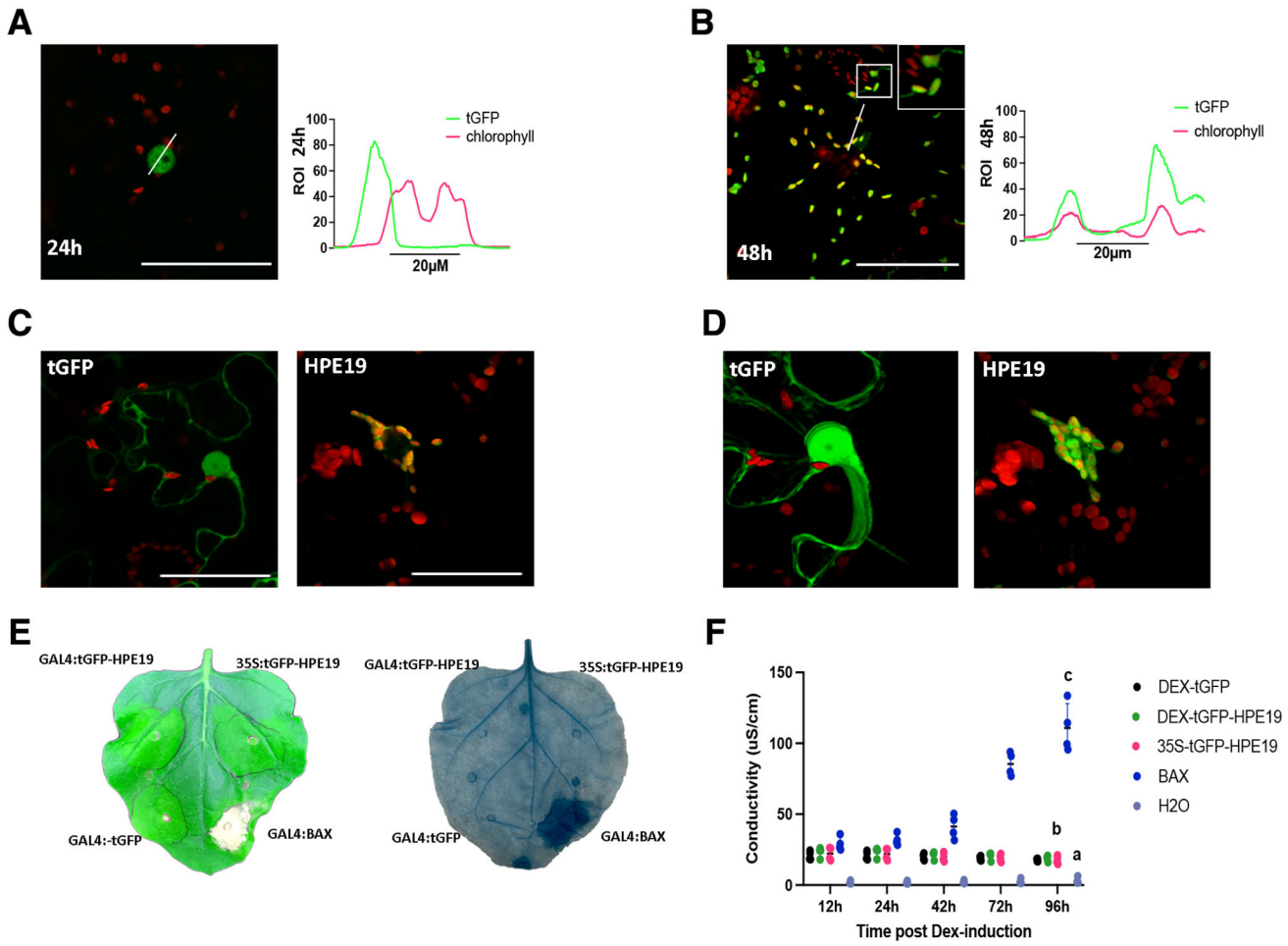

Fig. 4.

HPE19 exhibits dynamic nuclear chloroplast localization and alters immune responses in *Nicotiana benthamiana*. HPE19 lacking its signal peptide was cloned with an N-terminal fusion to TurboGFP (tGFP) under control of the GAL4 dexamethasone (Dex)-inducible promoter, transiently expressed in *Nicotiana benthamiana* and were visualized by confocal microscopy. Dex was applied 12 postinfiltration (hpi). **A**, HPE19 exhibits nuclear expression at 24 hpi. The left panel shows green fluorescent protein (GFP), the central panel includes chloroplast autofluorescence, and the right panel shows the intensity profile for tGFP and chlorophyll in the merged image. **B**, HPE19 primarily exhibits chloroplast localization at 48 hpi. Insert in the central panel shows chloroplast stromule-like projections. Right panel, tGFP and chlorophyll intensity profiles overlap in the merged image. **C**, Representative image of nuclei expressing tGFP (left) and chloroplasts surrounding nuclei carrying tGFP-HPE19 (right). **D**, Three-dimensional (3D) reconstructions of the tGFP control (left) and tGFP-HPE19 (right) 48 hpi illustrate chloroplast clustering around nuclei. 3D reconstructions were generated from 20 images. **E**, Overexpression of HPE19 fails to induce cell death. Left, macroscopic cell death observed 5 days postinduction with 2 μM Dex; right, cell-death visualized after trypan blue staining observed 5 days postinduction with 2 μM Dex **F**, Electrolyte leakage 12 to 96 hpi with 2 μM Dex. Individual dots represent values for four biological replicates per construct. Statistical differences were detected by a repeated

measures analysis of variance, and different groups were detected using a Tukey multiple comparison test. Different letters indicate significantly different groups of means at 96 hpi.

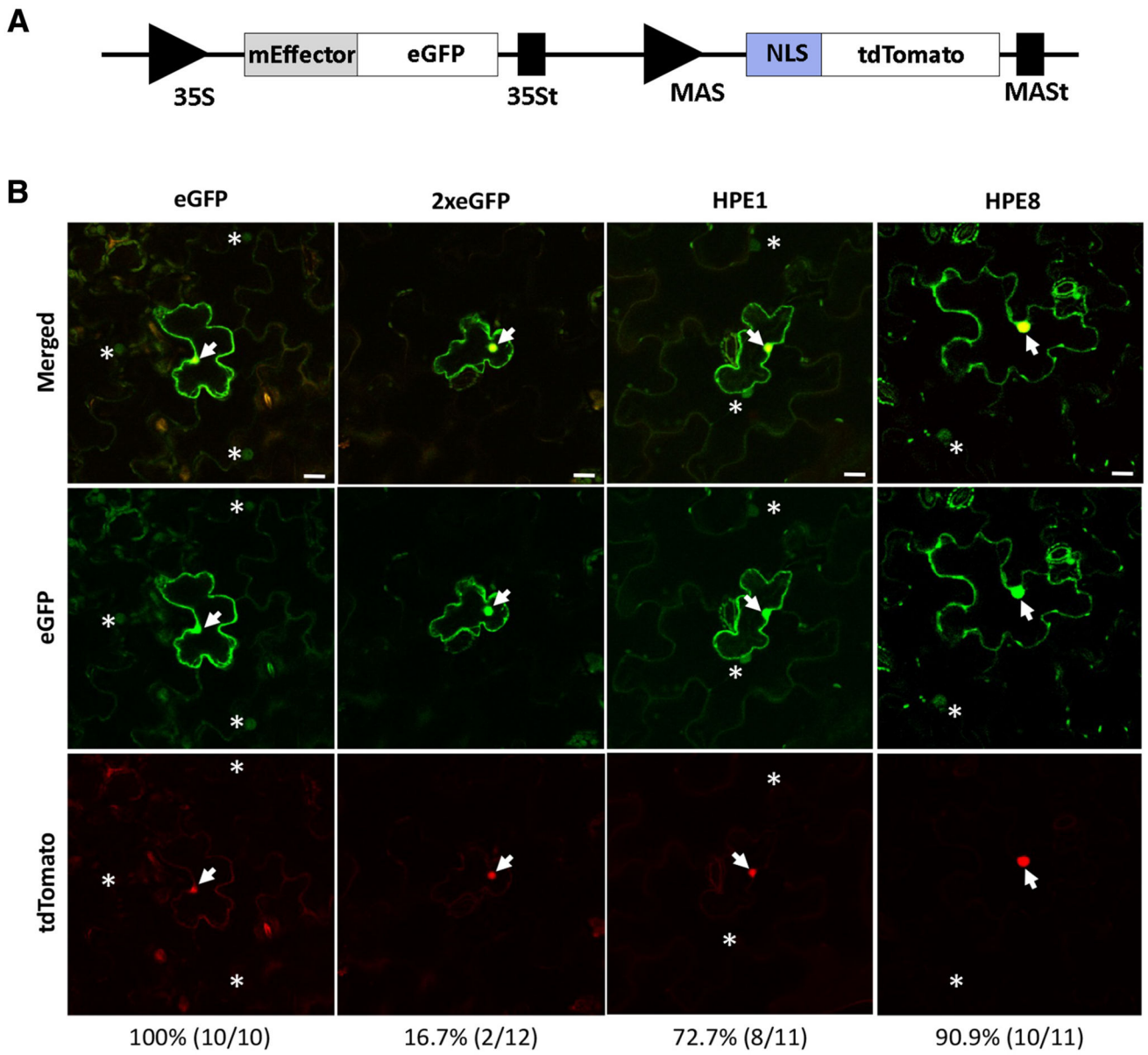

Fig. 5.

'*Candidatus* Liberibacter solanacearum' effectors are capable of cell-to-cell movement. **A**, Schematic representation of the construct used to test the ability of '*Ca*. L. solanacearum' effectors to move cell-to-cell. Mature effectors (mEffector) lacking their N-terminal signal peptide cloned with a C-terminal fusion to enhanced green fluorescent protein (eGFP) in a binary vector also containing tdTomato targeted to the nucleus. **B**, Confocal images show the diffusion of '*Ca*. L. solanacearum' mEffector-GFP fusion proteins in *Nicotiana benthamiana* epidermal cells 24 h after transient expression. The concentration of *Agrobacterium tumefaciens* for transient expression at optical density at 600 nm was 0.0005, which enabled single-cell transformation. The originally transformed plant cell exhibits both strong red fluorescence in the nucleus (arrows) and green fluorescence signals. Effector movement is determined by the detection of GFP but not tdTomato signal in cells surrounding the

transformed cell, indicated as asterisks. Scale bars = 20 μm. Numbers at the bottom indicate positive movement events out of total events observed.

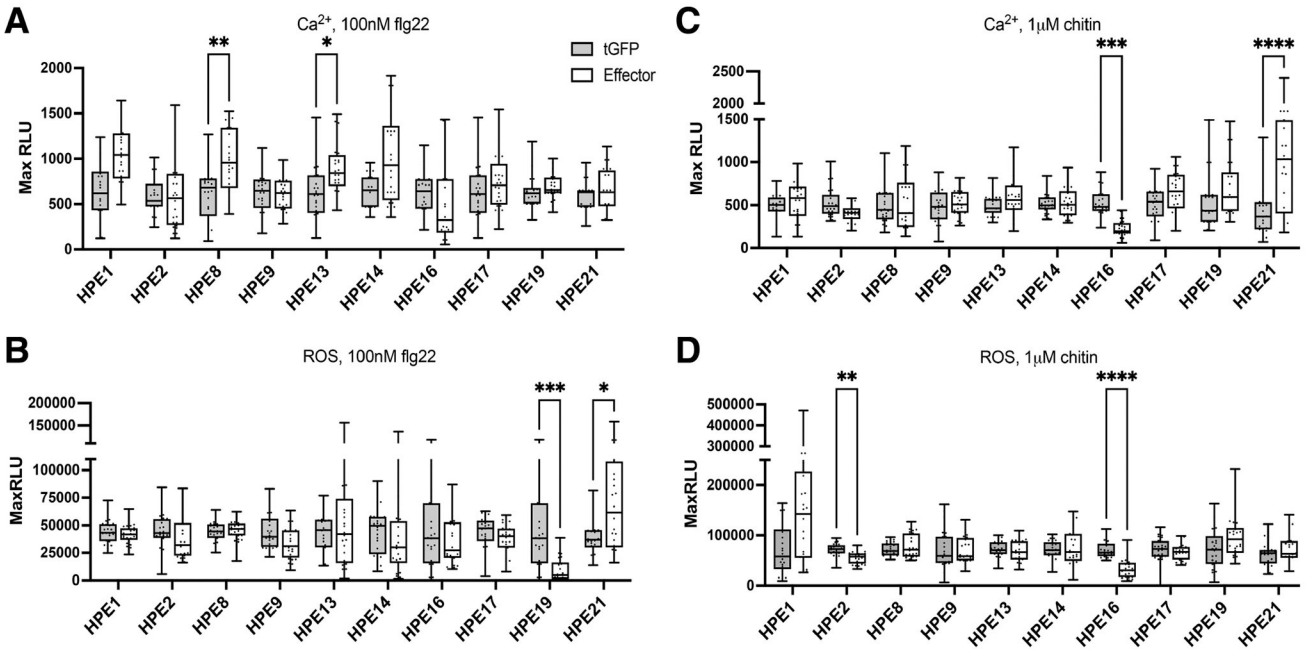

Fig. 6.

The majority of '*Candidatus* Liberibacter solanacearum' effectors do not alter plant immune responses to microbial features. Individual effectors were transiently expressed in *Nicotiana benthamiana* or the *N. benthamiana* Ca^{2+} reporter line SRLJ15 by *Agrobacterium* transient expression. *Agrobacterium tumefaciens* containing effector constructs were syringe-infiltrated on a single leaf side-by-side with the TurboGFP control. Inoculations were performed in triplicates. Samples were taken 24 h postinfiltration, were floated in water or Coelenterezine solution for 16 h, and were challenged with 100 nM flg22 or 1 μM chitin. **A to D**, Reactive oxygen species (ROS) production and Ca^{2+} accumulation were measured on a luminometer. The majority of '*Ca*. L. solanacearum' Sec-dependent effectors do not alter or weakly enhance the calcium cytosolic accumulation triggered by flg22 (A) or chitin (C) perception. The majority of '*Ca*. L. solanacearum' Sec-dependent effectors do not suppress the ROS production elicited by flg22 (B) or chitin (D). Statistical differences were detected by multiple Mann-Whitney tests. Multiplicity adjusted *P* values from the Holm-Sidak method were used to compute adjusted *P* values. One asterisk (*) indicates $P < 0.05$, two (**) $P < 0.005$, three (***) $P < 0.0005$, and four (****) $P < 0.00005$.

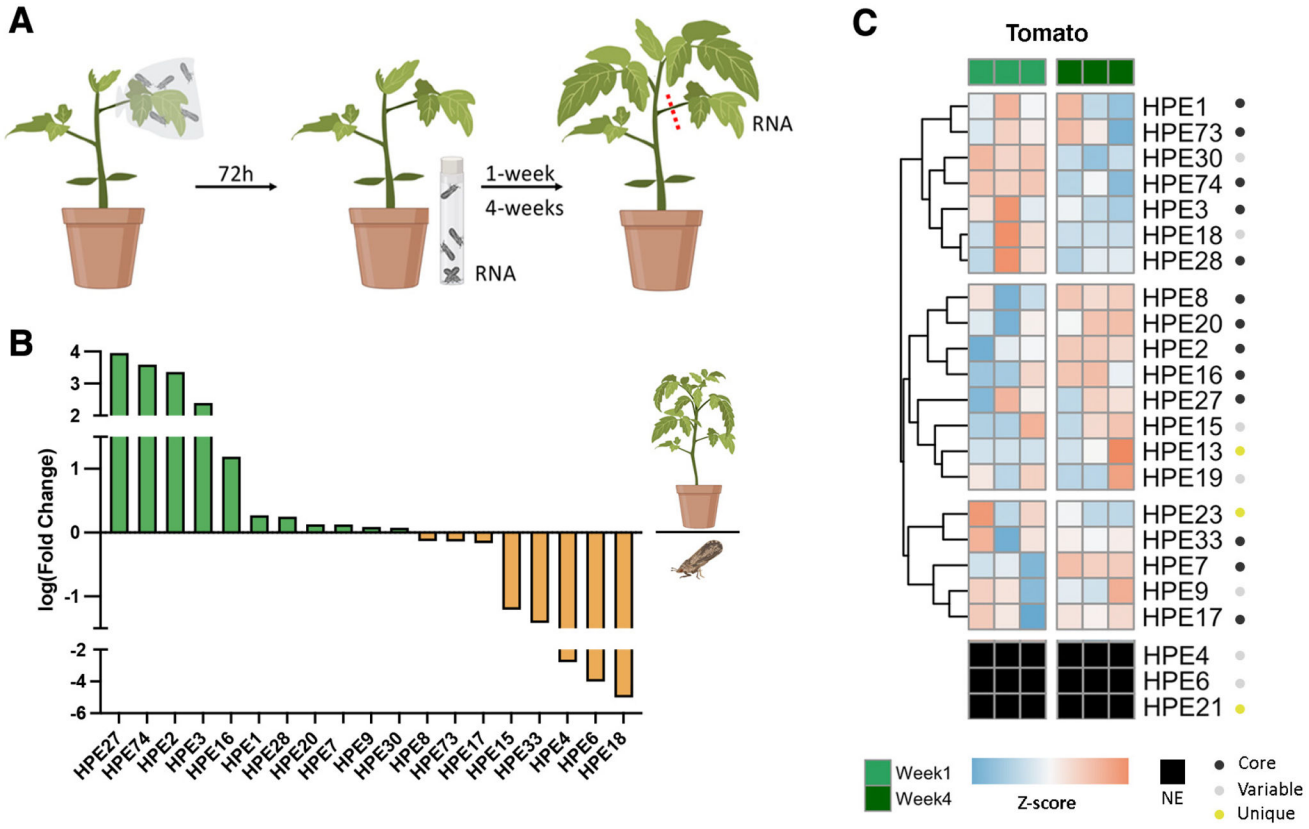

Fig. 7.

'*Candidatus* Liberibacter solanacearum' effectors exhibit dynamic expression according to organism and time. **A**, Experimental design for analyzing effector expression in psyllids (*Bactericera cockerelli*) and plants (tomato). Fifteen 1-day-old haplotype B psyllids were caged on the second leaf of 4-week-old tomato cv. Money Maker plants, using a mesh bag. Seventy-two hours later, psyllids were removed and stored at −80°C for RNA extraction. One or 4 weeks later, midrib tissue from the originally infected leaf was collected for each biological replicate ($n = 3$) **B**, Comparison of '*Ca.* L. solanacearum' core, variable, and unique effector expression in tomato and psyllids. '*Ca.* L. solanacearum' *glnA* was used for normalization. Samples of the same organism cluster together. The $^{\Delta\Delta}$Ct (cycle threshold) method was used to analyze effector expression, with results shown on a $\log_2$ scale. **C**, Effector expression changes over time. The heatmap shows one experiment with three biological replicates and two different timepoints (1 and 4 weeks). Sets of effectors with similar expression patterns are shown as distinct clusters. '*Ca.* L. solanacearum' *glnA* was used for normalization. The $^{\Delta}$Ct method was used to analyze effector expression, with results shown as a *Z* score. The pheatmap package in R was used to perform hierarchical clustering and visualize the results. NE = not expressed.